Journal of Colloid and Interface Science 614 (2022) 214–232

Contents lists available at ScienceDirect

Journal of Colloid and Interface Science

journal homepage: www.elsevier.com/locate/jcis

The changing face of SDS denaturation: Complexes of Thermomyces lanuginosus lipase with SDS at pH 4.0, 6.0 and 8.0

Helena Østergaard Rasmussen [a,b], Daniel T. Weltz Wollenberg [c,d], Huabing Wang [a,2], Kell K. Andersen [a,e,1], Cristiano L.P. Oliveira [a,b], Christian Isak Jørgensen [d], Thomas J.D. Jørgensen [c], Daniel E. Otzen [a,e,*], Jan Skov Pedersen [a,b,*]

[a] Interdisciplinary Nanoscience Center (iNANO), Aarhus University, Gustav Wieds Vej 14, 8000 Aarhus C, Denmark
[b] Department of Chemistry, Aarhus University, Gustav Wieds Vej 14, 8000 Aarhus C, Denmark
[c] Department of Biochemistry and Molecular Biology, University of Southern Denmark, Campusvej 55, DK-5230 Odense M, Denmark
[d] Novozymes A/S, Krogshøjvej 36, DK-2880 Bagsværd, Denmark
[e] Department of Molecular Biology and Genetics, Gustav Wieds Vej 10C, Aarhus University, 8000 Aarhus C, Denmark

GRAPHICAL ABSTRACT

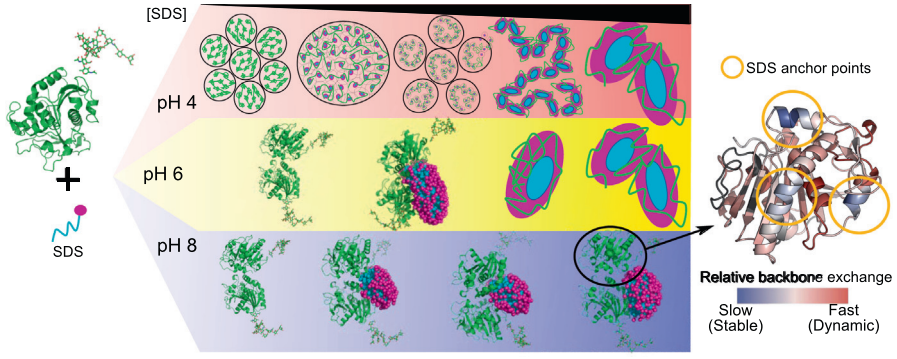

ARTICLE INFO

Article history:
Received 29 October 2021
Revised 16 December 2021
Accepted 29 December 2021
Available online 10 January 2022

Keywords:
Lipase
SDS
SAXS

ABSTRACT

Hypothesis: Lipases are widely used in the detergent industry and must withstand harsh conditions involving both anionic and zwitterionic surfactants at alkaline pH. *Thermomyces lanuginosus* lipase (TlL) is often used and stays active at high concentrations of the anionic surfactant sodium dodecyl sulfate (SDS) at pH 8.0, but is sensitive to SDS at pH 6.0 and below. We propose that enhanced stability at pH 8.0 results from a structurally distinct complex formation with SDS.
Experiments: We use small-angle X-ray scattering (SAXS) to elucidate structures of TlL:SDS at pH 4.0, 6.0, and 8.0 and further investigate the complexes at pH 8.0 using hydrogen/deuterium exchange mass spectrometry (HDX-MS).
Findings: At pH 4.0, large dense aggregates are formed at low [SDS], which become gradually less dense at

Abbreviations: TlL, Thermomyces *lanuginosus* lipase; CD, Circular dichroism; ITC, Isothermal titration calorimetry; SAXS, Small-angle X-ray scattering; CS, Core-shell; HDX, Hydrogen/deuterium exchange; SAX, strong anion exchange; LC, liquid chromatography; MS, Mass spectrometry; IFT, Indirect Fourier transformation; D_{max}, Maximum distance; CC, Compact cluster; RF, Random flight; H2, α-helix number 2; CBD, Cellulose binding domain; RL, Rhamnolipid; SANS, Small-angle neutron scattering.

* Corresponding authors.
E-mail addresses: dao@inano.au.dk (D.E. Otzen), jsp@chem.au.dk (J.S. Pedersen).
[1] Deceased.
[2] Present addresses: HW: Guangxi Key Laboratory of Enhanced Recovery after Surgery for Gastrointestinal Cancer, Clinical Laboratory Center, The First Affiliated Hospital of Guangxi Medical University, Shuangyong Road 6, 530021 Nanning, Guangxi Zhuang Autonomous Region, China. CLPO: Complex Fluids Group, Institute of Physics, University of Sao Paulo, Rua Do Matão, 1371, Butantã, São Paulo, Brazil.

https://doi.org/10.1016/j.jcis.2021.12.188

HDX-MS
Denaturation

higher [SDS], resulting in a core–shell structure. At pH 6.0, SDS induces a TlL dimer and forms a hemi-micelle along the side of the dimer. At higher [SDS], TlL adopts a core–shell structure. At pH 8.0, TlL forms a dimer with a SDS hemi-micelle but avoids a core–shell structure and maintains activity. Three helices are identified as SDS anchor points. This study provides important structural insight into the stability of TlL towards SDS under alkaline conditions.

1. Introduction

Enzymes are widespread in industry with diverse applications within the production of dairy products, food, beverages, textiles, and paper as well as personal care products and detergent formulations [1–3]. As of 2019, enzymes in detergent formulations made up the second largest market share of industrial enzymes after food and beverages [4]. Current detergent formulations contain several classes of enzymes such as proteases, amylases, lipases, and cellulases that contribute to laundering in different ways [3,5]. Among these, lipases help remove lipid stains by hydrolysis of ester bonds [1] and work in synergy with surfactants to enhance detergency [6]. Surfactants increase lipase activity through interfacial activation [7]. However, most detergents contain both anionic surfactants and alkaline buffers (pH $\sim$ 10), both of which tend to denature proteins. This poses additional challenges for the detergent enzymes [8]. In 1988, Novozymes A/S (at the time part of Novo Nordisk A/S) was the first company to launch a commercial lipase for the detergent industry [2]. The solution was called Lipolase® and was based on the *Thermomyces lanuginosus* lipase (TlL), which is resistant to both anionic surfactants and high pH [9]. TlL has a molar mass of 31.8 kDa, a catalytic triad of Ser(146), Asp(201) and His(258), a *N*-linked glycosylation site at Asn33 and a flexible lid over the active site (Res 86–92) [10–12].

We have previously studied the interactions between TlL and the anionic surfactant SDS at pH 4.0, 6.0, and 8.0 by Trp fluorescence, activity measurements, pyrene fluorescence, circular dichroism (CD) and isothermal titration calorimetry (ITC) [13]. That work forms the basis for the present study, and we therefore recapitulate the results in some detail. The most striking result was the strong dependence of lipase stability on pH. At pH 4.0, the protein was unfolded and inactivated by as little as 0.2 mM SDS (activity) to 0.5 mM SDS (Trp fluorescence) (Fig. 1AB). In contrast, TlL showed a much more robust profile at pH 6.0 and 8.0, with an initial increase in activity (peaking around 1.5–2.0 mM SDS) due to the surfactants opening up the lid, followed by a reduction in activity at higher [SDS], when TlL starts to unfold [7]. While activity and structure were both lost around 3 mM SDS at pH 6.0, residual activity remained up to 10 mM SDS at pH 8.0, and the protein remained folded (although destabilized) according to CD (Fig. 1B inset). Further evidence for radical changes in behavior at different pH values was uncovered by pyrene fluorescence, which indicated formation of SDS clusters or hemi-micelles on TlL from 0.05 and 1.5 mM SDS onwards at pH 4.0 and 6.0, respectively (Fig. 1C), but none at pH 8.0. ITC showed that TlL and SDS interact at all pH values but with much weaker interactions at pH 8.0 (Fig. 1D). This no doubt reflects changes in the net charge of TlL, computed to be + 18, −5 and −12 at pH 4.0, 6.0 and 8.0, respectively. Electrostatic attraction between anionic SDS and cationic groups on TlL leads to large exothermic signals. As described elsewhere [14], ITC data enable us to calculate the concentration of free SDS molecules ($[SDS]_{free}$) and number of bound SDS molecules per TlL monomer at selected transition points (Fig. 1D). We identified 4–5 such transition points at the three pH values. At the end of these transitions, TlL has bound around 107 SDS molecules at pH 4.0 and 6.0, but this declines precipitously to 23 SDS at pH 8.0 (Table 1). These numbers correspond to 1.08 g SDS/g TlL and 0.23 g SDS/g TlL, respectively. Proteins with intact disulfide bridges generally bind 0.6–1.0 g SDS/g protein [15]. Thus, TlL at pH 8.0 binds significantly less SDS than would be expected for a standard protein. Furthermore, our data indicate that the complexes formed between TlL and SDS are radically different at different pH values.

In the present study, we turn to a more comprehensive structural analysis to understand these pH-dependent variations in SDS interactions. Our approach is to determine low-resolution structures of the TlL:SDS complexes formed at all characteristic ITC transitions at pH 4.0, 6.0, and 8.0 by small-angle X-ray scattering (SAXS). SAXS is generally used to probe the mass, size, and overall structure of proteins and other macromolecules in solution. It is particularly useful for protein-surfactant complexes, as the contrast in SAXS data depend on electron densities, which vary considerably between TlL and the head groups of SDS on one side and the tail groups of SDS on the other. This contrast difference allows a thorough modelling of SAXS data and even to model large networks of complexes which lead to visible sample opacity.

We establish that at pH 4.0, large aggregated species of denatured TlL are formed at low [SDS]. At higher [SDS], the structures become smaller and less densely aggregated. Eventually, the classical core–shell (CS) structure is formed, where denatured protein is wrapped around one or more SDS micelles. This structure has also been found for a significant number of other protein and SDS complexes [16–22]. At pH 6.0, a dimer is induced at low [SDS]. At higher [SDS], the SAXS data indicate that a micelle is formed on one side of the dimer, and at the two highest [SDS], the CS structure is also observed. Finally, at pH 8.0, the TlL dimer is also initially induced, after which a SDS micelle forms on one side. At higher [SDS] up to saturation, additional SDS molecules add to the micelle but TlL remains dimeric and natively folded.

Since TlL remains folded at pH 8.0 and since basic pH is more relevant for the industrial application of TlL, we decided to investigate this structure further. While SAXS shows us the relative position of the dimer and hemi-micelles at pH 8.0, we cannot tell the orientation due to the relatively low resolution of SAXS and the high symmetry of the dimer at this resolution. Hydrogen/deuterium exchange measured by mass spectrometry (HDX-MS) allows us to extend our SAXS analysis by characterizing the structural dynamics of the SDS-induced TlL dimer which yields possible interaction sites within the complex.

Backbone amide hydrogens that form stable hydrogen bonds in a folded protein are protected against exchange with the solvent until the protecting hydrogen bonds break because of transient local or global unfolding. The deuterium uptake kinetics of a protein in deuterated buffer therefore directly reflect the continuous step-wise unfolding and refolding dynamics of the protein [23]. A protein–ligand association will typically induce a protection against exchange in the ligand binding site and HDX-MS has therefore long been utilized to probe local interactions in protein–ligand complexes (where ligands can be small molecules or other proteins) [24–26]. Detergents and amphipathic lipids are detrimental to the ESI-MS detection of peptides and proteins and several

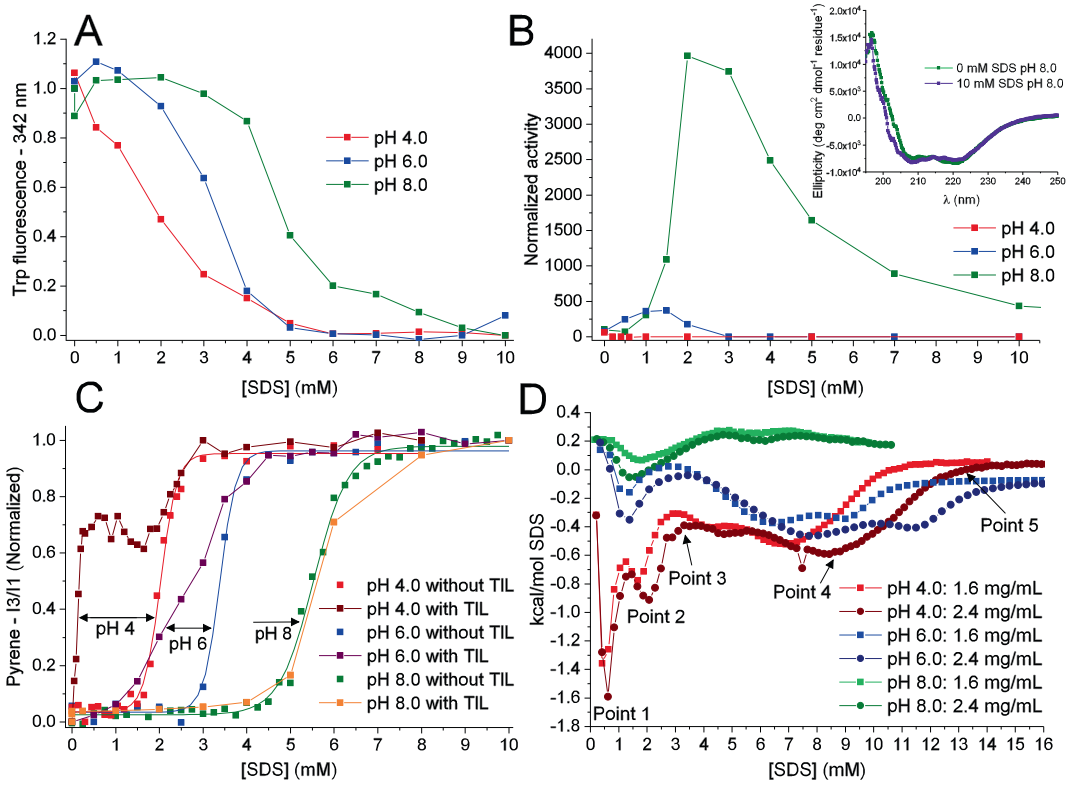

Fig. 1. TIL-SDS interactions measured by spectroscopy and calorimetry. Data replotted from [13]. A) Tryptophan fluorescence at pH 4.0, 6.0 and 8.0 as a function of [SDS]. B) Activity measurements at pH 4.0, 6.0 and 8.0 as a function of [SDS]. Inset shows CD spectra of TIL with and without 10 mM of SDS at pH 8.0. C) Pyrene fluorescence with and without TIL at pH 4.0, 6.0 and 8.0 as a function of [SDS]. D) ITC data at 1.6 and 2.4 mg/mL TIL at pH 4.0, 6.0 and 8.0 as a function of [SDS]. The five characteristic transition points are indicated for pH 4.0.

Table 1
Stoichiometry of binding od SDS to TIL at pH 4.0, 6.0, and 8.0 based on ITC. Table reprinted from [13]. The binding number and $[SDS]_{free}$ can be calculated from ITC data by plotting the [SDS] at transition points as a function of TIL concentration $[TIL]$ according to the equation $[SDS]_{transitionpoint} = n_{SDS} \times [TIL] + [SDS]_{free}$ [14].

	Binding number			$[SDS]_{free}$ (mM)		
Point	pH 4.0	pH 6.0	pH 8.0	pH 4.0	pH 6.0	pH 8.0
1	6.2 ± 1.2	0 ± 0	−14.2 ± 1.2	0.16 ± 0.1	1.39 ± 0	2.59 ± 0.06
2	21.2 ± 1.1	19.4 ± 3.8	10.6 ± 2.7	0.46 ± 0.08	1.85 ± 0.22	3.92 ± 0.15
3	32.0 ± 4.4	52.6 ± 0.2	17.20 ± 0.05	1.09 ± 0.35	3.75 ± 0.01	4.90 ± 0.01
4	36.0 ± 4.0	108.2 ± 7.4	23.2 ± 1.7	2.10 ± 0.32	3.42 ± 0.39	5.74 ± 0.07
5	107.2 ± 12.0			1.35 ± 0.9		

approaches have therefore been devised for minimizing their interference in HDX-MS experiments [27–34] . Here we present another approach based on a strong anion exchange (SAX) column for online trapping of the anionic surfactant SDS at quench conditions. This allows us to inject SDS-containing samples directly into the cooled LC setup, without prior SDS removal steps. In addition, by using the liquid handler to inject regeneration solvent onto the SAX column between sample injections we have a fully automated HDX setup for online SDS removal. To the best of our knowledge, this is the first demonstration of automated SDS removal implemented in an HDX-MS set-up based on reversed phase liquid chromatography (LC).

Our HDX-MS data show that SDS causes broad destabilization of the internal hydrogen bonding network of TIL at pH 8.0, which reaches a constant level above 1.6 mM for 2 mg/mL TIL. However, a broad distribution of relative exchange values confirms our preceding observations that TIL does not unfold even at the highest [SDS]. Instead, we even detect localized patterns of reduced exchange on parts of the surface of TIL upon addition of SDS. The localized sites of reduced exchange include the active side lid as well as two other sites with features such as hydrophobic patches and positive charges that provide anchor points for SDS binding. Our analysis provides novel insight into the great spectrum of structures that can be formed between TIL and anionic surfactants and provides a structural explanation for TIL's significant levels of residual activity at high [SDS] at pH 8.0.

2. Materials and methods

2.1. Materials:

TRIS (≥99.9%) and SDS (≥99.0%) were from AppliChem (Darmstadt, Germany). *Themomyces lanuginosus* lipase (TIL) was provided by Novozymes A/S as a liquid that was diluted and extensively dialyzed against MilliQ at 5 °C for 24 h. Furthermore, small amounts of precipitate were removed by centrifugation. TIL was stored at −80 °C and the concentration was determined by absorbance using the molar extinction coefficient of 37275 M^{-1} cm^{-1}. For HDX-MS H_2O was prepared locally by filtering demineralized

water on a milli-Q IQ7000 equipped with LC-Pak UHPLC filter. All other chemicals were of reagent grade and purchased from MERCK (Kenilworth, US).

2.2. Tryptophan fluorescence, activity assays, CD, pyrene fluorescence, ITC:

Data are replotted and summarized from [13], where the details of the individuals techniques can be found.

2.3. SAXS:

SAXS data were obtained on a modified laboratory-based NanoStar SAXS instrument from Bruker AXS (Karlsruhe, Germany) at iNANO (Aarhus University) [35]. The instrument has been flux optimized with homebuilt scatterless slits [36] that made it possible to reduce the number of pinholes from three to two. Data are measured as intensity ($I(q)$) as a function of the modulus of the scattering vector $q = 4\pi \sin(\theta)/\lambda$), where $\lambda = 1.54$ Å is the wavelength of the X-rays from the Cu source and 2θ is the angle between the incident and scattered X-rays. The samples were measured for 1800 s (0.5 h) at 25 °C with a concentration of 2.0 mg/mL TlL in 10 mM Tris buffer. The buffer was also measured and subsequently subtracted from the data using the SUPERSAXS package (C. L. P. Oliveira and J. S. Pedersen, unpublished). This package was also used to convert all data to absolute scale ($I(q)$ in cm^{-1}) by measuring a MilliQ water sample at 20 °C as a standard.

The theoretical SAXS signal from high-resolution structures in terms of PDB files were done using the method described in [37,38]. The Debye equation is used for calculating the scattering on absolute scale and a hydration layer is added in terms of dummy atoms representing the water molecules close to the surface of the protein. Structure factors for aggregates were included using the decoupling approximation [39], where the scattering amplitude is calculated using the distance, d, from the center of mass of the protein and hydration shell to the atoms (dummy atoms) with a single sum of $\sin(qd)/(qd)$. Expressions for the structure factor of a random flight (RF) and compact cluster (CC) are given in [40] and [41], respectively. The compact cluster structure factor included size polydispersity in terms of a Schulz distribution see e.g. [39]. Additionally, a hard-sphere (HS) structure factor was applied when fitting the dimer model. The HS structure factor describes inter-particle repulsions, which gave a minor, but significant, improvement when data were modelled using the dimer structure.

Addition of glycosylation group was done by first finding the average mass of a glycosylation, as the mass of the particular glycosylation was not known. The program GLYCOSYLATION in the ATSAS package [42] was used to convert the average mass to a realistic composition of carbohydrate groups which was then produced and manually attached close to the glycosylation site (N33) using PyMOL [43]. The used glycosylation has a mass of 2.5 kDa and is branched at two points. SAXS is a low-resolution technique and therefore not sensitive to the specific chemical composition of the glycans as well as the mass, when the glycosylation is much smaller than TlL.

The core–shell (CS) form factor expressions on absolute scale are the same ones as given in the SI of [17] and also used in [16,44,45]. The approach uses concentrations, volumes and corresponding electron densities of protein and surfactant head and tail groups, respectively, as constraints in the modelling. Furthermore, $[SDS]_{free}$ found by ITC was used for calculating the amount of SDS in the complexes. From the structural fitting results, stoichiometries of the complexes can therefore also be obtained. The models were optimized by conventional weighted least-squares fitting [46].

Data for 3.2 mM SDS at pH 6.0 and [SDS] > 1.6 mM at pH 8.0 were modelled by the PDB structure together with Monte Carlo generated points for SDS. The home-written program was based on the methods described in [37,47–49]. Uniformly distributed by Monte Carlo points were first generated and a tri-axial core–shell structure with super-ellipsoidal shape parameter t = 3 was used for selecting points for the core and the shell, respectively and this gave an initial representation of the SDS structure [50]. This structure was placed at origo and the protein was represented by the dimer with the glycosylation on each of the monomers (from PDB entry: 1EIN). When the protein overlapped with the CS structure, the corresponding Monte Carlo points were removed, and this could give a protein structure with a hemi-micelle on one or two sides of the protein structure. The volume of the core was estimated from the number of points and the point density, and the aggregation number was obtained by dividing the core volume by the volume of a C12 chain (353 $Å^3$). The shell contains both SDS headgroups and solvating buffer. An excess scattering length corresponding to the electron densities of C12 tails and heads were assigned to the Monte Carlo points in the core and in the shell, respectively. Similarly, the appropriate excess scattering length of a typical protein was assigned to the atoms/points of TlL and the scattering of a hydration layer was added.

A random search procedure was used for optimizing the parameters in the model. The varied parameters were the radius of the core, the axis ratio in two other directions, and the shell thickness. Additionally, the position and angle of the protein were optimized. Neither the total SDS concentration nor $[SDS]_{free}$ from ITC were implemented directly in the model, which made it necessary to adjust the initial structure, so it approximately agreed with the stoichiometry from ITC. Several starting models were used, however, some of them gave poor fit to the data, and those that agreed well with the data were quite similar. Due to the randomness in the search procedure, the final results were obtained by performing ten simulations with the same starting parameters for each SAXS data sets. The average of these ten simulations is reported as the final parameters and the uncertainties are calculated as standard deviations of these ten simulations.

2.4. HDX-MS:

Purified TlL was buffer exchanged into 10 mM TRIS at pH 8.0 by spinning at 14.000 × g in a 10 kDa spin filter until the solvent was exchanged 4 times by volume. TlL was then recovered and the concentration was adjusted to 20 mg/mL.

Working with surfactants in mass spectrometry applications poses specific challenges in terms of ion suppression. Handling surfactant samples becomes even more critical with the use of reversed phase LC-MS due to possible alteration of column chemistry and blockage. HDX provide an additional significant challenge, in that any time spend on sample preparation after the exchange has been quenched should generally be performed as fast as possible (within minutes) at low pH and low temperature. This is to minimize the loss of isotopic labeling referred to as back exchange. To address this, we utilized the difference in charge type between SDS (-) and our analyte (+) at low pH to trap and remove SDS in an on-line and automated setup by fitting a short, strong anion exchange (SAX) column in our cooled LC. In addition, by using urea as denaturant the minimum exchange rate is shifted from pH 2.5 to pH 3 achieving more efficient disulfide bond reduction with TCEP [51,52]. This setup, described in more detail below, is effective at preventing blockage and maintaining chromatographic performance up to at least 0.29 μmol of SDS per injection (40 μL at 7.3 mM) which was the largest amount used in this study.

Hydrogen deuterium exchange was performed in 10 mM TRIS buffer at pH 7.82 and 20 °C in the presence of 0 mM, 1.6 mM, 4.6 mM, 6.1 mM and 7.3 mM SDS by 10-fold dilution of the 20 mg/mL TlL stock into one of the exchange buffers [53]. Quench was performed by diluting the exchange solution 1/3 into 1 °C quench solution containing 4 M urea and 0.5 M TCEP for a final pH of 2.93 at 1 °C. After mixing, the quenched solution was injected into the 1 °C cooled LC for online SDS-removal, digestion and desalting for 10 mins at 0.2 mL/min with solvent A (0.3 % v/v formic acid in water) before chromatographic separation. SDS was removed by passing the injected sample over a Sperisorb SAX Guard Column with dimensions 4.6 mm × 30 mm, a particle size of 5 μm, and a pore size of 80 Å (Waters). The SAX column was placed in the flow path after the injection loop, but before the protease column. Digestion was carried out using a dual protease column pepsin/protease XVIII (w/w, 1:1; 2.1 × 30 mm) at 10 °C (NovaBioAssays Inc., Woburn, MA). The peptides resulting from the digestion of deuterated TlL were trapped and desalted on a reversed-phase trap column (Van Guard Acquity UPLC BEH C18 1.7 μm trap column, Waters, Milford, MA). Subsequently, the peptides were separated by reversed-phase chromatography using an analytical column (BEH C18 2.1 × 50 mm 1.7 μm, Waters). The LC gradient was 15–40 % B in 12 min at 0.L ml/min with Solvent Solvent B being 0.3 % (v/v) formic acid in acetonitrile. HDX was performed on a PAL-RTC liquid handler (Trajan, Morrisville, NC). The SAX column was regenerated after each injection by injecting 3 ml of 0.1 M hydrochloric acid and 90% acetonitrile in H_2O across the column and directly to waste. HDX-MS measurements were carried out on a maXis II equipped with ETD (Bruker Daltonik GmbH, Bremen, Germany) [54]. Two LC-MS/MS peptide mapping runs were done using CID to identify peptides and their retention times before HDX-MS. Further details on the HDX-MS data analysis are available in supporting information.

3. Results

3.1. SAXS shows TlL to be primarily a monomer in solution at pH 4.0, 6.0 and 8.0

We start out with SAXS analysis of native TlL at pH 4.0, 6.0, and 8.0 (Fig. 2) at 2.0 mg/ml, comparing them with a PDB structure of TlL in, respectively, the closed (PDB: 1DU4) and the open conformation (PDB: 1EIN). Before addition of SDS, TlL should be in the closed conformation. However, the calculated scattering curves of the open and closed conformation were basically indistinguishable (Fig. S2), *i.e* SAXS is not sensitive enough to detect the movement of the lid. Hence, we decided to use the same PDB structure for TlL throughout the analysis. The PDB structure does not include any glycosylation, but TlL is known to have one glycosylation site at Asn33 [12]. Therefore, a glycosylation group was added to Asn33 manually (see M&M for details) and the PDB structures with and without glycosylation were fitted to the data (Fig. 2) considering also the scattering contribution from the hydration layer of the protein. Addition of the glycosylation group significantly improved the fit, decreasing the χ^2-value for pH 4.0 from 1.27 to 1.09, for pH 6.0 from 4.47 to 1.04 and for pH 8.0 from 3.47 to 1.15. Thus, the PDB structure with the added glycosylation was used in subsequent analysis. The fit parameters for glycosylated TlL (Table 2) also lead to a protein concentration very close to the actually used 2.0 mg/mL at all pH values. For pH 4.0, it was necessary to have a fraction of the protein as a dimer, as the mass was slightly higher than a pure monomer. The dimer structure factor describes the structures as a dimer of the individual components with a certain separation. On average, a complex consists of 1.2 monomers (N_{prot}), which means that the sample primarily consists of monomers, but

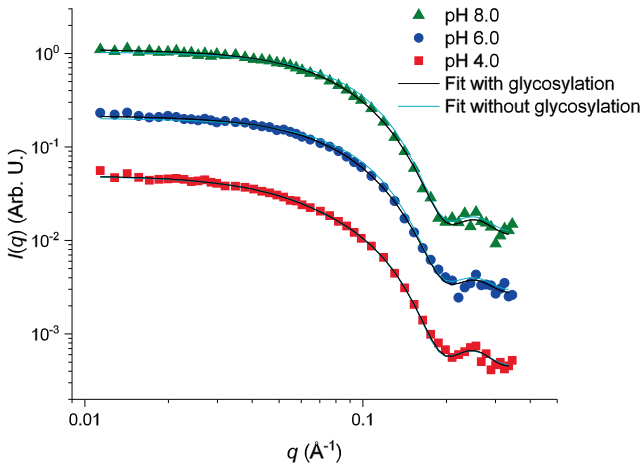

Fig. 2. SAXS data and fit of TlL without SDS at pH 4.0, 6.0 and 8.0. The fits are shown for the scattering from the PDB structure (PBD entry: 1EIN) with and without an added glycosylation group.

a minor fraction (ca. 35% of the total protein mass) is in the dimeric state. In conclusion, the crystal structure represents the structure in solution and TlL is primarily a monomer at all pH values with around 65 % of the total mass at pH 4.0 and 100 % at pH 6.0 and 8.0

3.2. At pH 4.0 TlL forms large complexes at low [SDS] and classic core–shell structure at high [SDS]

SAXS data were measured for all the transition points found in ITC, each of which represents a distinct part of the unfolding. Thus, the progression of structures during unfolding can be followed by measuring and modelling data at [SDS] corresponding to each of the transition points. It should be noted that the last transition point of ITC data is the saturation point just before the signal plateaus at which stage additional SDS will go into free micelles. As we only use [SDS] up to the saturation point, we would not expect any contribution from free micelles. We start with pH 4.0. Fig. 3A shows SAXS data for SDS-free TlL and TlL at an [SDS] corresponding to each of the five ITC transitions points. Clearly, these curves are quite different, underlining the significant changes occurring during unfolding. SAXS data for SDS alone are shown in Fig. S3A for comparison. The first step was to use an indirect Fourier transformation (IFT) as developed by Glatter [55] to calculate the $p(r)$ functions, *i.e.* histograms of pair distances within the particle weighted by the product of the electron density contrasts at the given points. The $p(r)$ function provides model-independent parameters such as the maximum distance, D_{max}, and information about the overall shape. Furthermore, the radius of gyration, R_g, and the forward scattering intensity, *I(0),* are also obtained through the IFT where the latter can be used to calculate the overall mass. The $p(r)$ functions are displayed in Fig. 3B, while Table 3 shows R_g and a rough estimate of the number of protein monomers in an oligomer/aggregate calculated from *I(0)* where the scattering from the SDS is neglected (# Monomers IFT). In the used SAXS setup, it is only possible to probe distances up to approximately 40 nm. Thus, when the $p(r)$ functions at 0.6, 1.9 and 3.3 mM SDS have D_{max} values higher than 40 nm, these are not precise values, but shows that the complexes are larger than 40 nm. This is also seen in the data in Fig. 3A, where the curves have not started to level out for the scattering vector modulus q approaching zero, but still have a large slope at low q. Above 3.3 mM SDS, the size of the complexes starts to decrease and for 8.7 mM, D_{max} is similar to that of TlL without any SDS (Fig. 3B). As regards shape, it is seen that 0.6, 1.9 and 3.3 mM are close to spherical, as the $p(r)$ function is almost sym-

Table 2
Parameters for TIL-SDS complexes at pH 4.0-8.0 obtained by fitting the data with the scattering from a monomer (PDB entry: 1EIN) with an added glycosylation group. *c* (mg/ml) is the fitted TIL concentration, $\rho_{hydration}$ is the scale of the scattering contribution from the hydration layer represented by dummy atoms around the protein. This is usually between 0.3 and 1.0 for a protein. N_{prot} is the number of TIL on average per complex and D_{prot} is the center-to-center distance between the two monomers in the dimer. (f) The parameter was fixed during fitting.

	χ^2	c (mg/mL)	$\rho_{hydration}$	N_{prot}	D_{prot} (Å)
pH 4.0	1.09	1.97 ± 0.02	0.77 ± 0.07	1.18 ± 0.01	56 ± 2
pH 6.0	1.04	2.02 ± 0.01	0.46 ± 0.03	1.00 (f)	–
pH 8.0	1.15	2.079 ± 0.009	0.44 ± 0.03	1.00 (f)	–

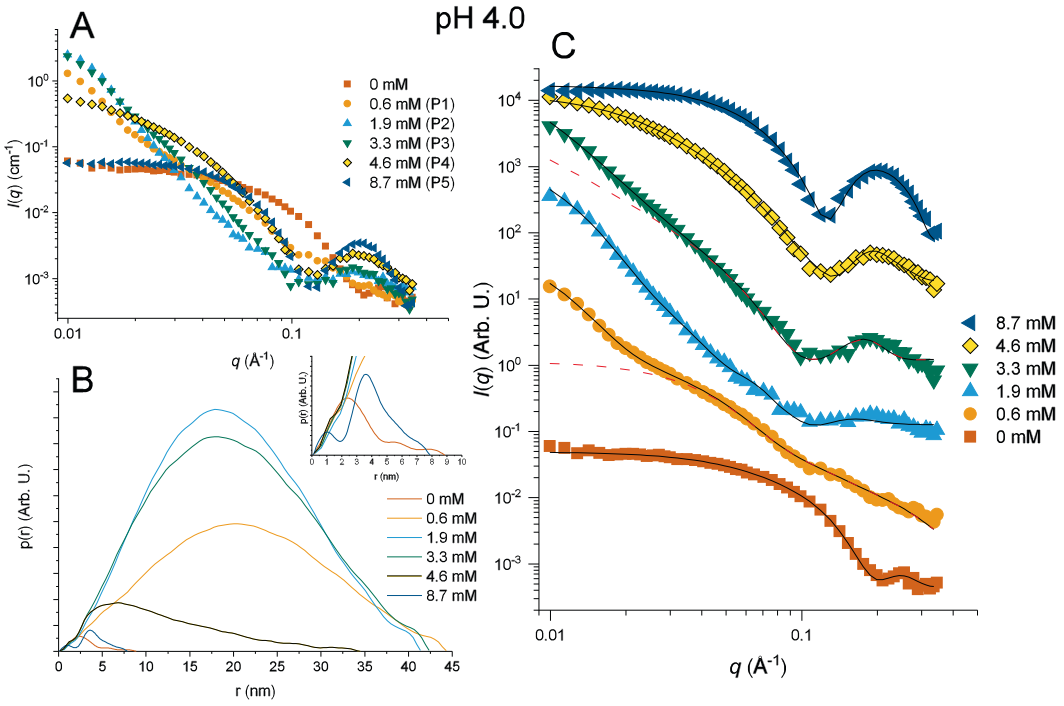

Fig. 3. SAXS data, $p(r)$ functions and fits for TIL:SDS complexes at pH 4.0. A) SAXS data overlaid. *P*1-5 in the parentheses indicate the ITC transition point. B) $p(r)$ functions calculated from data in A). Inset shows zoom in from 0 – 10 nm. C) Stacked SAXS data with fits from the modelling. Black solid lines show the final fit and red stippled lines show fits for 0.6 and 3.3 mM without the extra CC structure.

metrical and not particularly broad (Fig. 3B), unlike the case for oblate particles. At 4.6 mM, the complexes are more elongated as the maximum of the $p(r)$ is skewed to the left. Furthermore, there is a small shoulder around 1 nm, which generally arises from the CS structure [56] (inset Fig. 3B), which is even more pronounced at 8.7 mM. These CS features are especially pronounced for SDS alone (Fig. S3B).

3.3. SAXS modelling reveals compaction of the complexes decreases as a function of [SDS]

To aid the reader, we introduce in Fig. 4 a sketch of the models obtained from our SAXS models at pH 4.0, whose construction is described below. Fig. 4 also provides an overview of the Trp fluorescence, activity and hemi-micelle and cmc region which were found by pyrene fluorescence (Data in Fig. 1). The hemi-micelle and cmc regions are defined as the concentration range in which the transition occurs with and without TIL, respectively.

For the modelling of the individual curves between 0.6 and 8.7 mM SDS, the first step was to look for characteristic features that could point to the right model. The bump from the CS form factor is seen around q = 0.2 Å^{-1} at 1.9, 3.3, 4.6, and 8.7 mM SDS. Therefore, a CS model was the starting point for these curves as described below. However, we start with **0.6 mM SDS**, for which there is no CS bump. When comparing TIL alone and with 0.6 mM SDS, it is found that the intensity differs significantly in the intermediate q region (*i.e.* q = 0.04 – 0.1 Å^{-1}), where the tertiary structure of the monomer contributes. This indicates that the original globular fold has been broken down into smaller structural elements. To model this, an α-helical fragment of 3.2 kDa (29 aa) was used to mimic the smaller structured regions of TIL. Furthermore, structure factors were added to describe the aggregation of this fragment. The structure factor called compact cluster (CC, see M&M) was used to describe the relatively close packing of these fragments. This structure factor describes a spherical structure with size polydispersity that contains homogenously distributed defined particles inside, in this case in the form of the α-helical fragments. Each cluster consists of around 22 fragments which add up to 2.2 TIL monomers on average (N_{prot}, Table 3). However, this model is unable to describe the low-q region adequately, as seen in Fig. 3C, where the fit with one CC is depicted as the red stippled line. To achieve the sharp increase at low q, we included another CC factor, *i.e.* we model not a single cluster but a cluster of clusters. This supercluster contains around 64 of the original clusters (Fit Fig. 3C, Table 3, sketch Fig. 4B).

At **1.9 mM SDS**, the SAXS data contain the CS bump at q = 0.2 Å^{-1} and have a large slope that can be described by the

Table 3
IFT and selected fitting results for TlL:SDS complexes at pH 4.0. The results are organized in groups of primary unit, primary aggregation, super aggregation and calculated output to underline the hierarchical structure of the models. All fitting parameters and results can be found in Table S2, where fixed parameters relating to polydispersity, hydration and structure factor effects are included.

[SDS] (mM)	0.6	1.9	3.3	4.6	8.7
# Monomers of protein IFT[a]	73.8 ± 0.8[*]	123.9 ± 0.9[*]	118 ± 1[*]	17.1 ± 0.3	1.56 ± 0.01
R_g (Å) IFT[b]	165.3 ± 0.5	152.4 ± 0.3	155.2 ± 0.4	100 ± 2	29.9 ± 0.2
Modelling					
Model	N terminal fragment + 2 × CC	CS + CC	CS + RF + CC	CS + RF	CS + RF
χ^2	4.05	6.41	8.54	4.66	3.00
Primary unit					
R_{core} (Å)[c]	–	5.6 ± 0.3	6.8 ± 0.3	9.51 ± 0.04	13.3 ± 0.1
D_{shell} (Å)[d]	–	26 ± 1	24 ± 1	14.9 ± 0.2	7.7 ± 0.1
ε [e]	–	2.0 (f)	2.0 (f)	2.0 (f)	2.0 (f)
N_{agg} [f]	–	4.2 ± 0.7	7.6 ± 1.0	20.4 ± 0.3	55.4 ± 1.3
$M_{micelle}$ (kDa)[g]	–	5.9 ± 1.8	6.1 ± 0.8	15.7 ± 10.7	16.6 ± 1.1
# SDS_{bound} /Mon[h]	–	23 ± 5	40 ± 1	41 ± 1	104 ± 2
$[SDS]_{free}$ (mM)[i]	–	0.46 (f)	0.8 (f)	2.0 (f)	2.0 (f)
Primary aggregation					
$N_{micelle}$ [j]	–	$1.4 \times 10^3 \pm 0.2 \times 10^3$	1000 (f)	22.1 ± 0.6	1.69 ± 0.05
$D_{micelle}$ (Å)[k]	–	–	40 ± 3	42 (f)	42 (f)
N_{prot} [l]	22.0 ± 0.6	–	–	–	–
R_{prot} (Å)[m]	28.8 ± 0.4	–	–	–	–
Super aggregation					
N_{super} [n]	64 ± 6	–	5.9 ± 0.3	–	–
R_{super} ;R_{super} ; R_{clust} (Å)[o]	139 ± 3	121 ± 2	43 ± 2	–	–
$\sqrt{R^8/R^6}$ (Å)[p]	284 ± 6	280 ± 5	85 ± 4	–	–
Calculated output					
# Monomer[q]	142 ± 14	261 ± 88	1135 ± 25	11 ± 7	0.9 ± 0.1

[a] Number of monomers calculated from the *I(0)* obtained by the IFT procedure.
[*] Denotes that these are minimum values as the complex size is outside the experimental range.
[b] Radius of gyration obtained by the IFT procedure.
[c] Radius of the core (Fig. 4F).
[d] Width of the shell (Fig. 4F).
[e] Axis ratio of the core (see sketch Fig. 4F).
[f] Aggregation number of SDS molecules per complex/micelle.
[g] Mass of protein per micelle.
[h] Number of bound SDS molecules per TlL monomer defined as ($N_{agg} \times N_{micelle}$)/#Monomer.
[i] Concentration of free SDS molecules (parameters found by ITC analysis).
[j] Average number of micelles in a complex.
[k] Distance between the centers (see sketch in Fig. 4F).
[l] Number of *N*-terminal fragments in average per complex.
[m] Center-center distance between *N*-terminal fragments (see *R* on sketch Fig. 4B).
[n] Number of spherical structures in a CC that are added either on top of another CC structure (0.6 mM) or a CS structure (3.3 mM).
[o] Distance between the N_{super} spherical structures (See sketch Fig. 4BCD).
[p] Intensity weighted radius of spherical structures in the CC structure.
[q] Number of monomers per complex.

CC structure factor (Fit Fig. 3C, Table 3, sketch Fig. 4C), *i.e.* a compact cluster of core–shell structures, which leads to a satisfactory fit. At **3.3 mM SDS**, the CS bump is even more pronounced, and some aggregation is seen. However, the initial slope of the curve at intermediate *q* is too low to be described by a CC. Therefore, a random-flight (RF, see M&M) structure factor is used. An RF structure factor describes the scattering of an ensemble of a number of particles in random flight configurations with a certain step length between the particles. Note that for CS, the RF structure factor describes a random flight of micelles on the surface of which the protein is distributed. This combination of CS and RF factors describe most of the data at 3.3 mM, but there are still some discrepancies at low *q* as seen from the fit with the red stippled line in Fig. 3C. In this region, the slope starts to increase, and thus we need to also include the CC structure factor to obtain a good fit (Fit Fig. 3C, Table 3, sketch Fig. 4D). Finally, at **4.6 and 8.7 mM SDS**, a classical CS structure with a RF structure factor nicely models the data (Fit Fig. 3C, Table 3, sketch Fig. 4EF), with a significant decrease in the number of micelles per complex as we go from 4.6 to 8.7 mM SDS. In general, the number of SDS bound per TlL monomer (# SDS_{bound}/Mon (defined as ($N_{agg} \times N_{micelle}$)/#Monomer), Table 3) is in good agreement with ITC binding numbers (Table 1), which therefore supports the low-resolution structures found through SAXS modelling.

3.4. At pH 6.0 TlL shows no aggregation before forming core–shell structures and forms dimeric hemi-micellar structure at low to intermediate [SDS]

We next turned to pH 6.0 and collected SAXS data (Fig. 5A) and calculated the corresponding $p(r)$ functions (Fig. 5B) for four transition points identified by ITC. The low D_{max} values make it clear that the samples are not aggregated at any [SDS], unlike the situation at pH 4.0. However, there is still a difference in mass as TlL is primarily in the form of a dimer at 1.4 and 3.2 mM (Table 4). The shapes are close to spherical as judged by the relatively symmetric $p(r)$ functions. Important for our modelling, the CS shoulder with a minimum around 2 nm is only seen at 7.3 and 10.8 mM SDS.

At **1.4 mM SDS**, 0 SDS molecules should be bound according to ITC (Table 1). This number is most likely an artefact of possible peak overlap in ITC, but still emphasizes that few SDS molecules are bound at this concentration. This prompted an attempt to describe the data as a dimer without SDS molecules, which turned out to be an adequate description (Fit in Fig. 5C, Table 4, sketch Fig. 6B). This was in good agreement with earlier reports of TlL

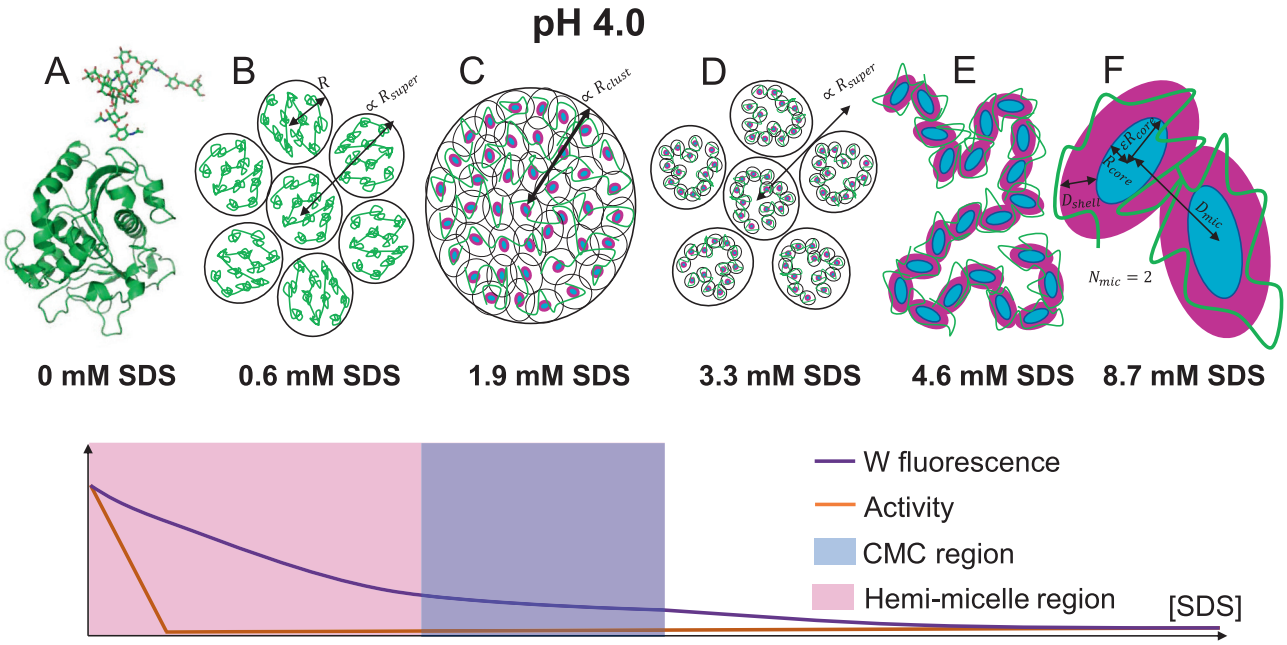

Fig. 4. Sketches of models that describe the SAXS data for TIL:SDS complexes at each SDS concentration at pH 4.0. A) TIL in its native form in cartoon representation with glycosylation. B) TIL is completely unfolded and forms compact cluster (CC) as the primary unit. A fragment of TIL is represented by the green small clusters. These are densely packed to form a complex with a certain radius (R) as shown by the black circles. On top of this, the complexes also form larger CC with a radius $\propto R_{super}$. C) SDS starts to form small core–shell (CS) structures with TIL. The cyan color represents the tail groups of SDS, the magenta color represents the headgroups of SDS, and the green lines represent TIL. These structures are densely packed to form a CC with a radius $\propto R_{clust}$. TIL is spread among many CS structures and the shell has a high content of buffer. D) CS structures of SDS and TIL are less densely packed with the primary unit showing a random flight (RF). There is also some super aggregation in form of CC that show a radius $\propto R_{super}$. E) Less dense CS structures with a RF aggregation of in average 22 CS complexes on one structure. F) CS complex formed at saturation. A TIL monomer is here shown to be split between two micelles with a RF aggregation. The bottom panel gives an overview of Trp fluorescence, activity, and pyrene fluorescence (which gives cmc and hemi-micelle region) using data from Fig. 1.

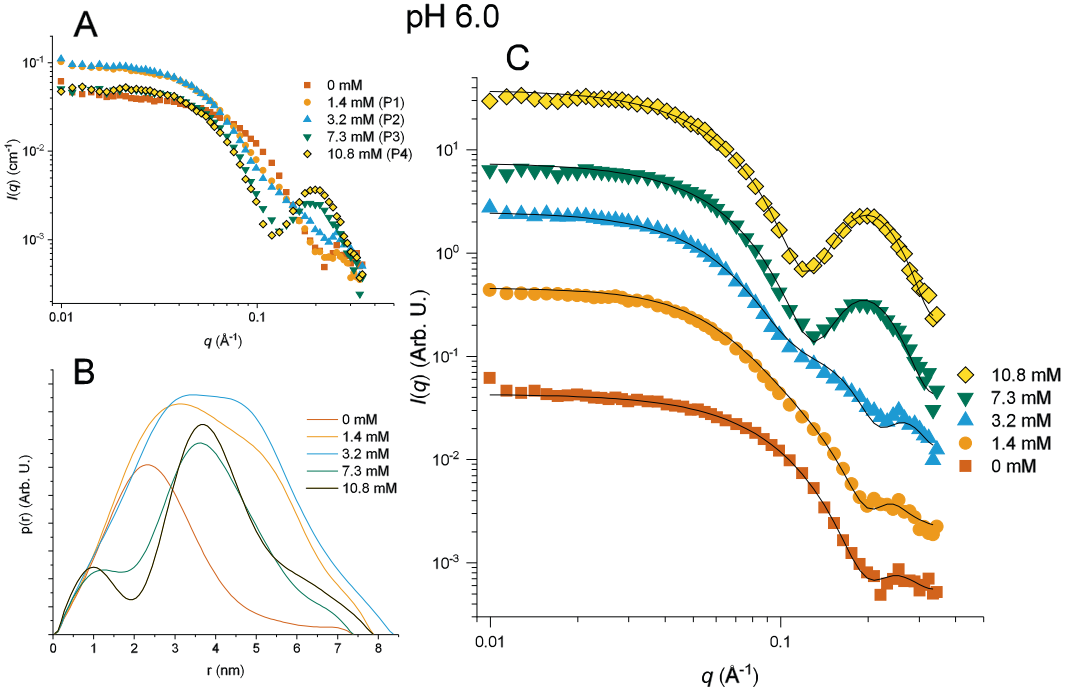

Fig. 5. SAXS data, $p(r)$ functions and fits for TIL:SDS complexes at pH 6.0. A) SAXS data overlaid. $P1$-4 in the parentheses indicate the ITC transition point. B) $p(r)$ functions calculated from data in A). C) Stacked SAXS data with fits from the modelling shown as black lines.

forming dimers in solution through hydrophobic contacts between the two lid regions in the open conformation [57]. At **3.2 mM SDS**, 19 SDS molecules should be bound per monomer according to ITC (Table 1), and here the dimer model had to be expanded to allow SDS to form a rim at the interface between the two monomers. This model was developed based on four observations. 1: IFT analysis showed TIL to be primarily dimeric (Table 4). 2: ITC showed substantial binding of SDS (Table 1). 3: TIL retained enough activity

Table 4
IFT and selected fitting results for TIL:SDS complexes at pH 6.0. The results are organized in groups of primary unit, primary aggregation and calculated output to underline the hierarchical structure of the models. All fitting parameters and results can be found in Table S3 that include parameters relating to hydration, polydispersity and structure factor effects.

[SDS] (mM)	1.4	3.2	7.3	10.8
# Monomers of protein IFT[a]	2.307 ± 0.009	2.48 ± 0.01	1.39 ± 0.01	1.421 ± 0.009
R_g (Å) IFT[b]	29.2 ± 0.1	30.5 ± 0.1	27.8 ± 0.2	29.4 ± 0.2
Modelling				
Model	Dimer	Dimer + hemi-micelle	CS + RF	CS + RF
χ^2	6.08	10.3 ± 1.76	4.43	3.17
Primary unit				
c(TIL) (mg/mL)[r]	2.41 ± 0.02	1.68 ± 0.02	–	–
R_{core} (Å)[c]	–	13 (f)	12.0 ± 0.1	13.0 ± 0.2
Dis_{core} (Å)[s]	–	–	3.6 ± 0.4	2.0 ± 0.3
D_{shell} (Å) [d]	–	5 (f)	11.1 ± 0.2	8.6 ± 0.2
ε [e]	–	–	2.0 (f)	2.0 (f)
ε_{core_y} [t]	–	2.2 (f)	–	–
ε_{core_z} [u]	–	2.2 (f)	–	–
N_{agg} [f]	–	78 ± 4	41.0 ± 1.0	52.0 ± 2.4
$M_{micelle}$ (kDa)[g]	–	–	21.6 ± 1.7	14.2 ± 1.5
$[SDS]_{bound}$ (mM)[v]	–	2.1 ± 0.1	3.8 (f)	7.3 (f)
# SDS_{bound} /Mon[h]	–	39 ± 2	59 ± 3	109 ± 7
$[SDS]_{free}$ (mM)[i]	–	–	3.5 (f)	3.5 (f)
Primary aggregation				
$N_{micelle}$ [j]	–	–	1.45 ± 0.07	1.68 ± 0.07
$D_{micelle}$ (Å)[k]	–	–	38 (f)	36 (f)
Calculated output				
# Monomer[q]	–	–	1.0 ± 0.1	0.8 ± 0.1

[a] Number of monomers of protein calculated from the *I(0)* obtained by the IFT procedure.
[b] Radius of gyration obtained by the IFT procedure.
[r] Fitted TIL concentration.
[c] Radius of the core.
[s] Displacement of the core.
[d] Width of the shell
[e] Axis ratio of the core (see Fig. 6E).
[t,u] Axis ratio of the hemi-micelles in the dimer + hemi-micelle model in *y* and *z* direction, respectively.
[f] Aggregation number of SDS molecules per complex/micelle.
[g] Mass of protein per micelle.
[v] Concentration of bound SDS fitted in the dimer + hemi-micelle model.
[h] Number of bound SDS molecules per TIL monomer defined as ($N_{agg} \times N_{micelle}$)/#Monomer.
[i] Concentration of free SDS molecules (parameters found by ITC analysis).
[j] Average number of micelles in a complex and
[k] Distance between the centers (see in Fig. 6E).
[q] Number of monomers per complex. All results for the dimer + hemi-micelle model (including χ^2 values) are the average value of ten simulations and the uncertainty is the standard deviation.

to be predominantly natively folded (Fig. 1B). 4. SAXS data did not contain a pronounced bump from the CS form factor (Fig. 5A). In the model, the radius of the hydrophobic core and shell with head groups could be fitted along with the axis ratio in two directions. Furthermore, the position and angle of the protein could also be fitted. By moving the protein to the side, the micelle would be located on one side, as micelle and protein could not overlap in the modelling algorithm. With this relatively large number of structural parameters, it was necessary to apply random Monte Carlo simulation steps to seek out possible structures (See M&M). For each structure, ten simulations were run with the same starting parameters and the average of these ten simulations is reported as the final parameters with uncertainties calculated as standard deviations. This procedure shows the robustness of the modelling, as the parameters are similar, and the final structures look almost identical. At 3.2 mM SDS, the binding number of around 38 (2 × 19, Table 1) could only be reached with the micelle on the side rather than all around the interface (Fit in Fig. 5C, Table 4, sketch Fig. 6C). The fit for 3.2 mM SDS gives an average χ^2 value of 10.3, which is higher than for the rest of the structures. A possible explanation is that the structure is not exclusively a dimer. Indeed, $p(r)$ calculations show that the average structure consists of 2.5 monomers, so some trimers or tetramers are also present in the sample. However, this is difficult to model, as simulations would have to be performed on dimer and trimer separately followed by combining these curves to describe the final data. This would introduce many more parameters some of which would be ill-determined, rendering the analysis unfeasible. Locking the structure to a particular multimer by using a PDB structure as the starting point, is simply one of the limitations of the described modelling approach.

3.5. SAXS modelling shows a classical CS structure with core displacement at high [SDS]

The data for **7.3 and 10.8 mM SDS** show the bump for the CS form factor. However, the depth of the minimum is not as low as would be expected from a symmetric CS structure. Therefore, a displacement parameter of the core was introduced. This means that the protein is not uniformly distributed around the micelle, which can be due to residual structural elements such as disulfide bridges that keep parts of the protein more compact. This effect was mostly seen at 7.3 mM and only to a small extent at 10.8 mM SDS (Fit Fig. 5C, Table 4, sketch Fig. 6DE). The need to introduce this displacement also shows that even though it is possible to unfold TIL to the standard CS structure at pH 6.0, TIL is more stable than at pH 4.0 where displacement was not required in the modelling. Furthermore, it is seen that the number of bound SDS molecules per TIL monomer of, respectively, 59 ± 3 and 109 ± 7 (# SDS_{bound}/Mon in Table 4) are in good agreement with ITC data that shows

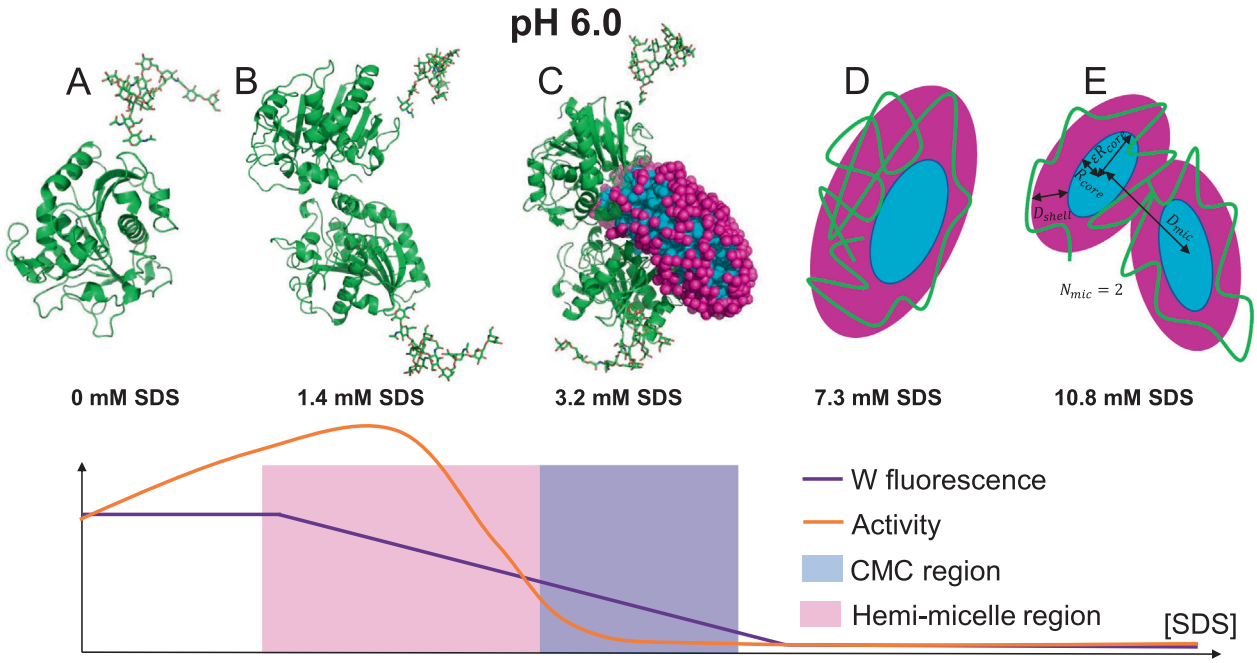

Fig. 6. Sketches of models that can describe the SAXS data for TIL:SDS complexes at each SDS concentration at pH 6.0. A) TIL in its native form in cartoon representation with glycosylation. B) SDS induces a TIL dimer. The SDS concentration is so low that SDS is not visible by SAXS. C) TIL still forms a dimer where more SDS is close to the interface forming a hemi-micelle. The cyan color represents the tail groups of SDS, and the magenta color represents the head groups of SDS. D) A CS complex is formed where the core is displaced to one side. One TIL monomer is shown to be on one SDS micelle. The green color represents TIL. E) CS complex at saturation where one TIL monomer is distributed onto two micelles. The bottom panel gives an overview of Trp fluorescence, activity, and pyrene fluorescence (which gives cmc and hemi-micelle region) using data from Fig. 1.

binding numbers of, respectively, 52.6 ± 0.2 and 108.2 ± 7.4, (Table 1). The binding number at saturation is the same as that seen at pH 4.0 (108.2 ± 7.4 *vs.* 107.2 ± 12.0) despite TIL having an overall positive charge at pH 4.0 and negative charge at pH 6.0. This can be explained by not only the electrostatics but also hydrophobic interactions determining the stoichiometry of TIL:SDS complexes. We have previously shown that an uncharged protein adopted the CS structure at high [SDS], indicating that hydrophobic interactions are of greater importance than electrostatic interactions in protein-surfactant systems [58].

3.6. TIL does not unfold at pH 8.0, but forms dimer complex with SDS

We finally turned to pH 8.0 where we recorded SAXS data at four ITC transition points at pH 8.0 (Fig. 7A). The $p(r)$ functions show that these samples are not aggregated (Fig. 7B) and that even at the highest [SDS], there is no shoulder/minimum around 1 nm, unlike for pH 4.0 and 6.0. We conclude that the CS structure is not formed at pH 8.0. Furthermore, the data show that a dimer is induced at the lowest [SDS] of 1.6 mM and is sustained at all concentrations (# Monomer IFT, Table 5). At **1.6 mM SDS**, ITC data indicate a negative binding number (Table 1) which we attribute to dimerization, since increasing protein concentration will increase dimerization and thus reduce the amount of possible SDS binding sites due to reduction in accessible surface area. We therefore fitted a dimer without SDS to the data as was done for the lowest [SDS] at pH 6.0. This was again found to be a sufficient description of the data (Fit in Fig. 7C, Table 5, sketch Fig. 8B). At **4.6–7.3 mM SDS**, the model with a PDB dimer and a rim of SDS was used to model the data employing a Monte Carlo simulation search. Data were fitted with SDS on either one or two sides of the dimer complex. To maintain the binding number predicted from ITC, the structures were best described with the SDS rim positioned only on one side (Fit in Fig. 7C, Table 5, sketch Fig. 8CDE). However, for 7.3 mM the binding number was large enough to be compatible with a structure having a hemi-micelle on both sides, but this could only be optimized to an average χ^2 value of 6.19 ± 0.48, which is significantly larger than the average χ^2 value of 4.15 ± 0.53 with the hemi-micelle only on one side.

3.7. HDX-MS reveals a constant TIL destabilization level above the cmc at which TIL remains natively folded

To further interrogate the dimeric structure observed in SAXS at pH 8.0, we utilized HDX to gain local information on structural stability at the various [SDS], measured as the extent of exchange (the greater the exchange, the lower the stability). Details of the HDX data set are provided in Table S1. Secondary structures in TIL are termed *H1* and *S1* for the first α-helix and β-strand in the sequence respectively etc. (full notation can be seen using chain A of PDB structure 1EIN).

The HDX-MS data allowed us to construct heatmaps visualizing the relative deuterium uptake along the TIL sequence at 0, 1.6, 4.6, 6.1, and 7.3 mM SDS (Fig. 9 and Fig. S4-S8 secondary structures were plotted using the Biotite python framework [59]). The relative deuterium uptake (relative deuteration) is the measured D-content of the peptide relative to the number of backbone amides in the peptide. At 0 mM SDS, the overall structure of TIL is rigid as most regions are strongly protected against isotopic exchange with the solvent as evidenced by the low deuterium uptake (<21%) in most of the peptides throughout the sequence after 50 min of exchange (Fig. 9). However, a few regions are less protected and these, more dynamic regions are the N- and C-terminal, the active site lid α-helix (*H2*), a small surface exposed α-helix (*H5*), a bend (A122-R126) in a surface exposed α-helix (*H3*) and several surface exposed loop regions (C36-A40, E56-D62, F188-L193, V203-E210, S224-R232, I238-A243). We attribute the dynamic behavior of the active site lid to an interconversion between the two conforma-

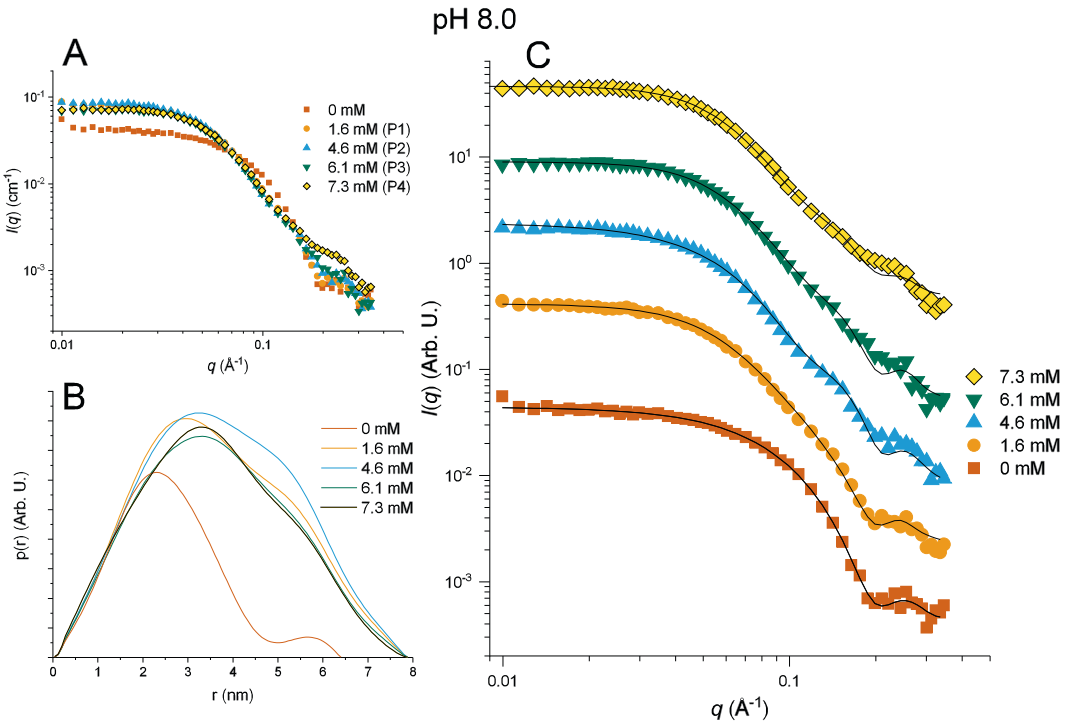

Fig. 7. SAXS data, $p(r)$ functions and fits for TIL:SDS complexes at pH 8.0. A) SAXS data overlaid. *P*1-4 in the parentheses indicate the ITC transition point. B) $p(r)$ functions calculated from data in A). C) Stacked SAXS data with fits from the modelling shown as black lines.

Table 5
IFT and selected fitting results for TIL:SDS complexes at pH 8.0. All fitting parameters and results can be found in Table S4 that include parameters relating to hydration and structure factor effects.

[SDS] (mM)	1.6	4.6	6.1	7.3
# Monomers of protein IFT[a]	2.136 ± 0.009	2.28 ± 0.01	1.975 ± 0.01	1.987 ± 0.009
R_g (Å) IFT[b]	28.29 ± 0.09	29.0 ± 0.1	28.2 ± 0.1	27.9 ± 0.1
Modelling				
Model	Dimer	Dimer + hemi-micelle	Dimer + hemi-micelle	Dimer + hemi-micelle
χ^2	2.50	8.45 ± 1.4	4.42 ± 1.10	4.15 ± 0.53
Primary unit				
c(TIL) (mg/mL)[r]	2.26 ± 0.01	1.73 ± 0.01	1.59 ± 0.02	1.63 ± 0.03
R_{core} (Å)[c]	–	11 (f)	12 (f)	13 (f)
D_{shell} (Å)[d]		5 (f)	5 (f)	5 (f)
ε_{core_y} [t]	–	1.7 (f)	1.5 (f)	1.47 ± 0.30
ε_{core_z} [u]	–	1.7 (f)	1.6 (f)	1.80 ± 0.35
N_{agg} [f]	–	35 ± 3	37 ± 4	54 ± 5
$[SDS]_{bound}$ (mM)[v]	–	0.94 ± 0.07	0.94 ± 0.09	1.39 ± 0.13
# SDS_{bound} /Mon[h]	–	17.5 ± 1.2	18.5 ± 2	27 ± 2

[a] Number of monomers calculated from the *I(0)* obtained by the IFT procedure.
[b] Radius of gyration obtained by the IFT procedure.
[r] Fitted TIL concentration.
[c] Radius of the core.
[d] Width of the shell.
[t,u] Axis ratio of the hemi-micelles in the dimer + hemi-micelle model in *y* and *z* direction, respectively.
[f] Aggregation number of SDS molecules per complex/micelle.
[v] Concentration of bound SDS fitted in the dimer + hemi-micelle model.
[h] Number of bound SDS molecules per TIL monomer defined as ($N_{agg} \times N_{micelle}$)/#Monomer. All results for the dimer + hemi-micelle model (including χ^2 values) are the average value of ten simulations and the uncertainty is the standard deviation.

tional states "lid open" and "lid closed". Furthermore, our results suggest that the α-helical lid region largely unfolds when it opens, rather than moving as a rigid body which would preserve internal hydrogen bonding. This interpretation is supported by molecular dynamics [60].

The relative deuterium uptake of peptides for each [SDS] at 50 min of exchange can be visualized by plotting the frequency of peptides at a given relative deuteration level (Fig. 10A). It shows there is an increase in the median of the relative deuterium uptake from 12.0 % to 24.2 % as we go from 0 to 7.3 mM SDS, showing that SDS destabilizes the protein structure. This destabilization of TIL due to SDS is expected as the melting temperature, T_m, of TIL decreases from 72 °C to 40 °C in 10 mM SDS [7,13].

The overall relative deuterium uptake increases from 0 mM to 1.6 mM SDS (12.0 to 16.5 %) and again from 1.6 mM to 4.6 mM SDS (16.5 % to 24.2 %), but largely stays constant between 4.6 mM and 7.3 mM SDS, indicating distinct destabilization

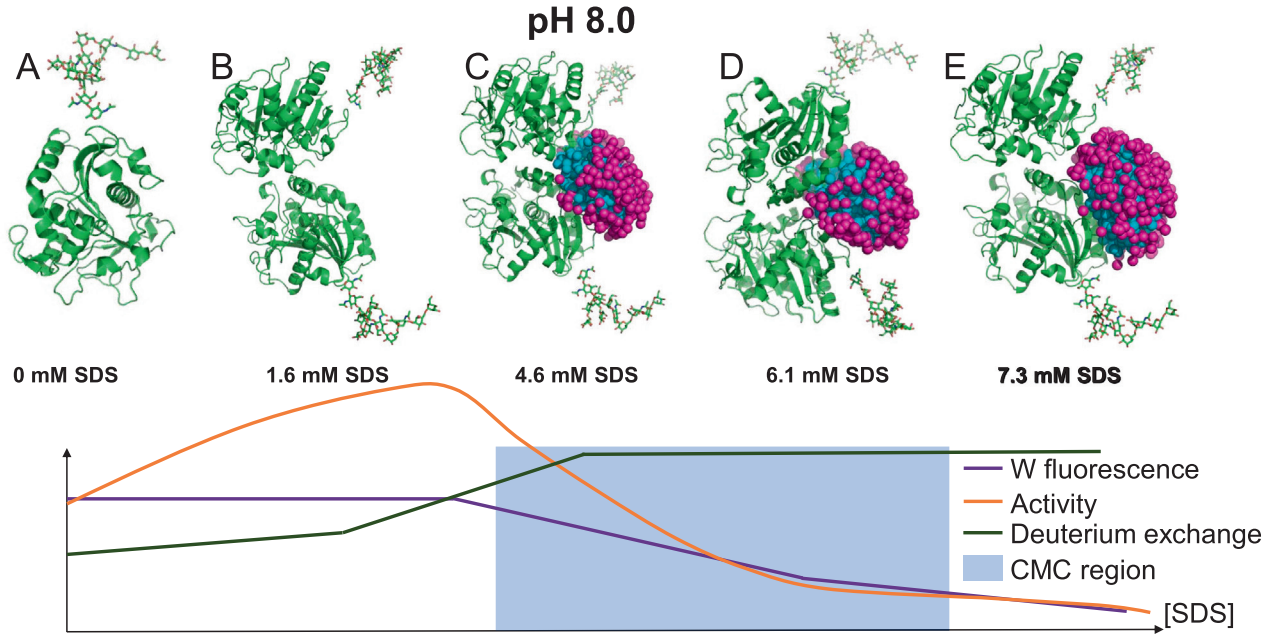

Fig. 8. Sketches of models that can describe the SAXS data for TIL:SDS complexes at each SDS concentration at pH 8.0. A) TIL in its native form in cartoon representation with glycosylation. B) SDS induces a TIL dimer. The SDS concentration is so low that SDS is not visible by SAXS. C-E) TIL dimer with SDS bound near the interface forming a hemi-micelle. The cyan color represents the tail groups of SDS, and the magenta color represents the head groups of SDS. The bottom panel gives an overview of Trp fluorescence, activity, and pyrene fluorescence (which gives cmc) using data from Fig. 1, as well as median relative deuterium uptake from HDX-MS data density plots in Fig. 10A.

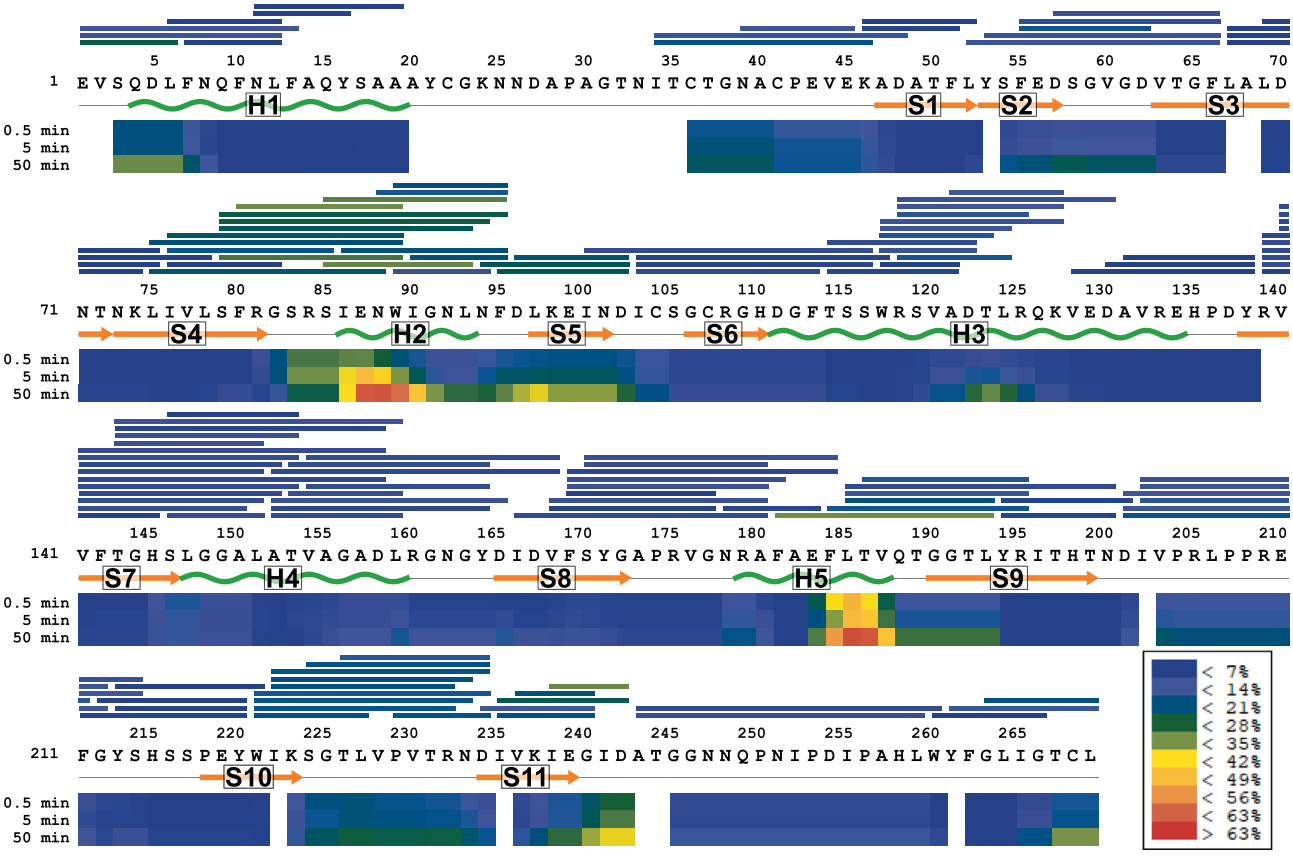

Fig. 9. Heatmap showing the relative deuterium uptake for each position in TIL for 0 mM SDS at 0.5, 5, and 50 mins of exchange as determined by the HDExaminer software. The bars above the sequence represent the measured peptides and the colors represent the relative deuterium uptake for that peptide. β-strands are numbered and marked by orange arrows, α-helices are numbered and marked by green waves. The secondary structure annotations were plotted using the Biotite python framework [59].

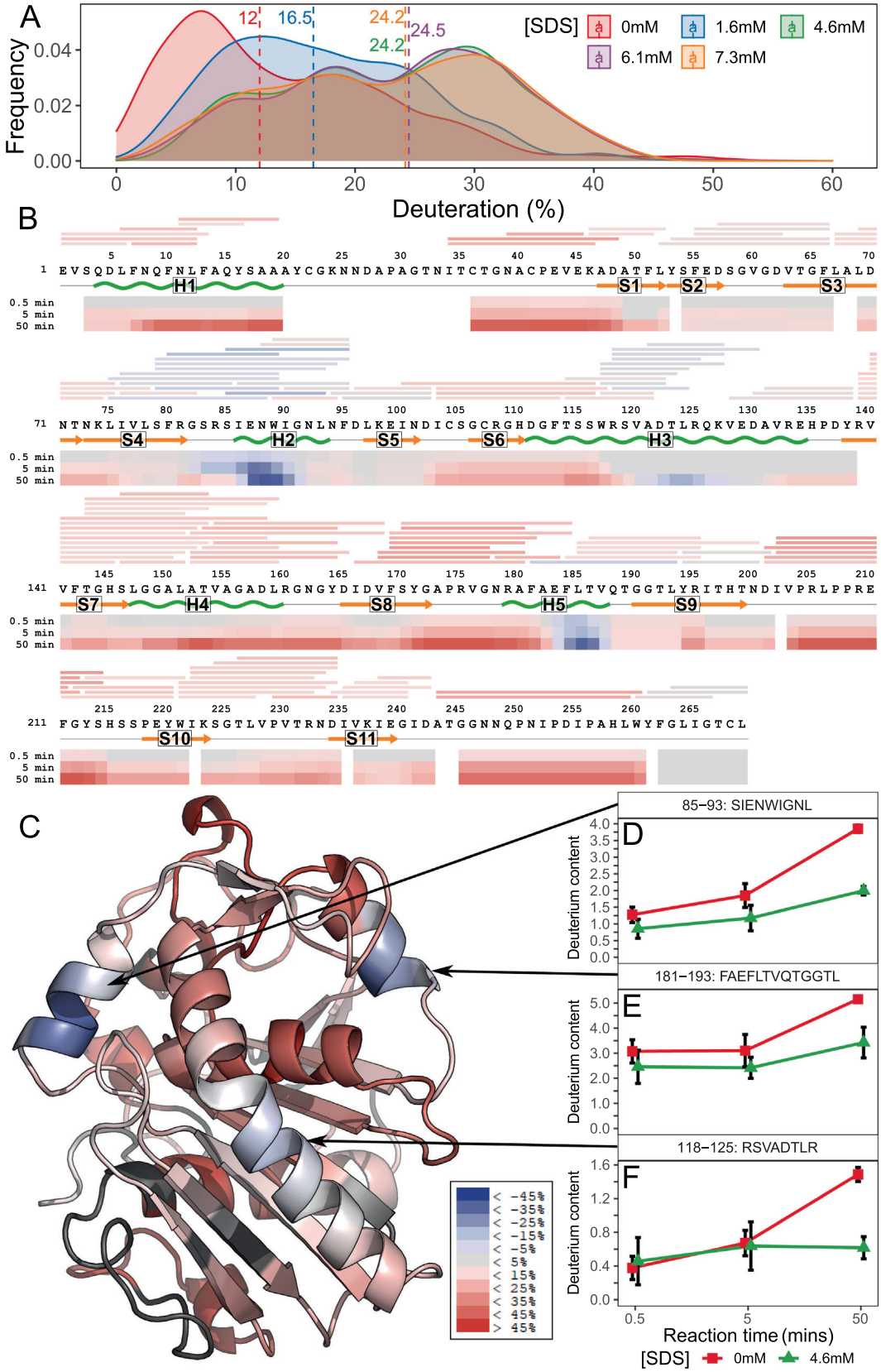

Fig. 10. (A) Relative deuterium uptake frequency plot for 50 min time point at 0 mM (red), 1.6 mM (blue), 4.6 mM (green), 6.3 mM (purple) and 7.1 mM (orange) SDS. The median relative deuteration percentage is indicated by vertical dashed lines. (B) Heatmap showing the average difference in deuteration for each position in TIL for 0 *vs* 4.6 mM SDS for 0.5, 5, and 50 mins. β-strands are numbered and marked by orange arrows, α-helices are numbered and marked by a green wave using Biotite python framework [59]. Only differences that are both greater than the global measurement error of 0.3203 and individually significant ($p \leq 0.05$) are shown. (C) TIL overlaid with HDX difference heatmap data from 0 *vs* 4.6 mM SDS at 50 mins of exchange. Black indicate no HDX coverage. Visual representation was created in PyMOL. (D-F) Uptake plots for peptides; ^{85}SIENWIGNL^{93} located in the lid region (*H2*), ^{181}FAEFLTVQTGGTL^{193} located at a small surface exposed α-helix (*H5*), and ^{118}RSVADTLR^{125} located at an α-helix bend (*H3*). Error bars indicate 95% confidence intervals. Identical time points are slightly offset for legibility.

regimes below and above the cmc (Fig. 10A). This is in line with the SAXS models which indicate distinct quaternary structures at 0 mM, 1.6 mM and above 1.6 mM of SDS, where the SDS hemimicelle is detected by SAXS. It is also evident from the HDX data that TlL retains the natively folded structure even at the highest [SDS], which is seen by the broad distribution of relative uptake levels with a tail towards low relative uptake even at 50 min of exchange (Fig. 10A). In addition, for 4.6–7.3 mM SDS there is progression in deuterium uptake from 0.5 min to 50 min of exchange showing that exchange remains slow. This provides further evidence that TlL is still folded.

3.8. HDX-MS identifies SDS anchor points

To determine which specific regions of TlL that are affected by SDS, difference heatmaps were made by subtracting the relative deuteration obtained in the presence of SDS from the relative deuteration level without SDS for each peptide at each exchange timepoint (Fig. 10B and S9-S12). By mapping the heatmap colors onto the 3D structure of TlL, the SDS-induced differential exchange is visualized in a structural context (Fig. 10C). Increased protection from exchange can either be caused by protein–protein interactions, SDS binding, allosteric effects or a combination of these.

Interestingly, at 4.6 mM SDS, *H2* (lid), *H3*, and *H5* have a lower deuterium uptake than in the absence of SDS (Fig. 10BC, compare green and red D-uptake curves in Fig. 10D-F). The difference in deuterium uptake is most pronounced at the longest exchange time (50 min) reflecting that the SDS-induced protection predominantly affects backbone amide hydrogens that are already protected to some extent because they are part of α-helices. Several other peptides covering *H2* (lid) and *H3* also show a decrease in exchange above 1.6 mM SDS. Uptake data for these and the peptides in Fig. 10D-F including all [SDS] are available in Table S5. Overall, SDS causes an increased stabilization of helices *H2*, *H3* and *H5*, while most other regions in TlL exchange more readily in the presence of SDS reflecting a general structural destabilization of TlL, as noted earlier.

To better understand what causes the protection of these sites, they were investigated in more detail. It was found that the decrease in deuterium uptake observed in *H2* (lid) coincides with an amphiphilic α-helix, for which the hydrophobic side is buried when the lid is closed and solvent exposed when the lid is open (Fig. 11A-B). Thus, opening provides a binding site for SDS which in turn stabilizes the lid in the open position. Two factors can directly explain the protection at the lid. First, the binding of SDS will cause water displacement from the site, potentially reducing the exchange rate by limiting access to solvent. Second, in the open state the lid helix is rotated close to 180° when comparing Fig. 11A (open) and Fig. 11B (closed). This rotation could increase stabilization of the open state interactions between residues that are otherwise solvent exposed in the closed state and the rest of the structure. *H5*, also protected in the presence of SDS, is part of a

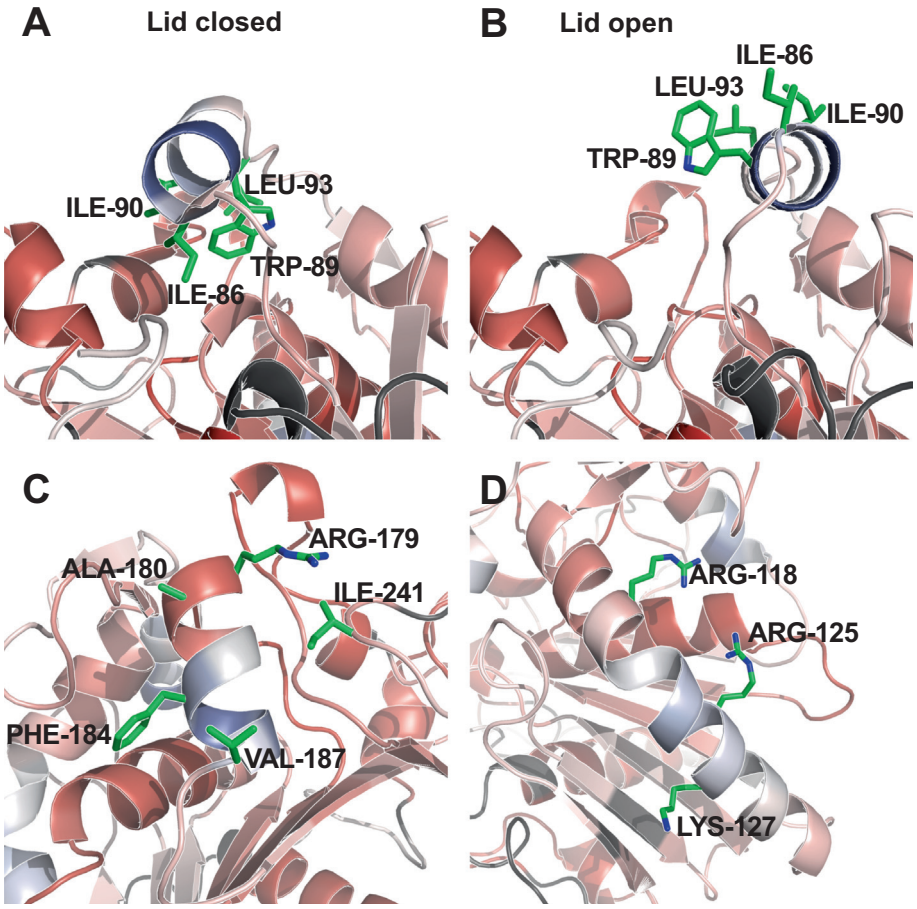

Fig. 11. Sites on TlL which show a reduction in deuterium uptake in the presence of SDS. Selected side chains are shown as sticks with carbon in green and nitrogen in blue. (A) TlL lid in closed state with hydrophobic *H2* (lid) residues rotated away from the solvent (PDB: 1DT3). (B) TlL *H2* (lid) in open state with hydrophobic residues rotated towards the solvent (PDB: 1EIN). (C) *H5* showing reduced exchange in the presence of SDS. *H5* contains a number of hydrophobic residues on the surface along with Arg179 and Ile241 in close proximity (PDB: 1EIN). (D) *H3* showing protection from exchange in the presence of SDS, the site is surrounded by positively charged sidechains. Representations were created in PyMOL.

hydrophobic patch on the surface, which is flanked by the surface exposed Arg179 (Fig. 11C). The long *H3*, which show reduction in exchange around positions R118-R125 in the presence of SDS, is not hydrophobic but does contain Arg118, Arg125 and Lys127, all with surface exposure (Fig. 11D). As all sites are hydrophobic and/or positively charged, they are most likely anchor points for SDS.

We note that, at the lower concentration of 1.6 mM SDS, only *H2* (lid) and *H5* show protection from exchange (Fig. S9). This indicates that *H2* (lid) and *H5* are part of the initial binding interface in the TlL:SDS complex, whereas protection of *H3* could be due to an expanding protein-SDS interface as the [SDS] increases.

4. Discussion

We have combined SAXS and HDX-MS to analyze the overall structural aspects and specific interactions between TlL and the anionic surfactant SDS. At all three pH values, SDS-free native TlL is primarily present as a monomer, but the response to increasing amounts of SDS differs strongly. At pH 4.0, large aggregates are formed already at the lowest [SDS] of 0.6 mM, leading to a milky suspension. These aggregates become smaller as [SDS] increases, until the CS structure is adopted with only 1.7 micelles and one monomer per complex. This stands in contrast to TlL:SDS complexes at pH 6.0 that initially form a dimer which binds more SDS before rearranging and adopting the CS structure with a displaced core (*i.e.* an asymmetric protein distribution). Thus, at pH 6.0 there are no large aggregates, and the asymmetry of the CS structure shows that the structure is more robust towards SDS denaturation. At pH 8.0, the structures of TlL:SDS complexes at low [SDS] resemble initial structures at pH 6.0, but they start to differ at higher SDS concentration where TlL does not rearrange to the CS structure, but instead remains a folded dimer that can bind an SDS hemi-micelle. HDX-MS data show that TlL is destabilized but not unfolded even at high [SDS] and identify interaction sites for the TlL:SDS dimer complex at pH 8.0. The protected sites coincide with hydrophobic patches and a cluster of positively charged side chains, making them likely anchor points for SDS.

4.1. Comparison of SAXS and HDX-MS data

At first glance, the structural progression observed in SAXS does not lend itself to an interpretation of the protection pattern in HDX. For instance, while SAXS identifies a dimer at 1.6 mM SDS, HDX shows two distant protected sites already at 1.6 mM SDS. In addition, there is no progression in protection for HDX between 4.6 mM SDS and 7.3 mM SDS, while SAXS show association of a growing number of SDS molecules to TlL. These apparent differences can likely be attributed to the fundamental difference in the way SDS is detected in HDX and SAXS, respectively. Initial binding of only a few SDS molecules will drive most of the reduction in HDX. Additional SDS molecules are more in contact with the hemi-micelle than the protein surface and will therefore have decreasing impact on HDX. In turn, protection is detected in HDX before enough SDS has associated to be detectable by SAXS. Furthermore, it should be stressed that the resolution of the SAXS complexes is not high enough to determine at what side of the dimer the hemi-micelle is situated. Therefore, we cannot directly compare the position of the hemi-micelle in the SAXS model to protected sites in HDX-MS. Instead, we can evaluate if the protected residues in HDX-MS are compatible with the overall structure with a hemi-micelle on one side. With this in mind, we can reconcile the HDX data with the SAXS structures. *H2* and *H5*, being the first sites to show protection in HDX, could be part of a protein–protein interface and/or a protein-SDS interface. However, as noted in Results, these regions have cationic and hydrophobic patches making them likely anchor points for SDS. Protection of multiple sites is compatible with the SAXS models, given the large surface area which is either covered by the SDS hemi-micelle or participating in dimer formation. This leaves *H3*, which only show SDS-induced protection above 1.6 mM SDS. This indicates that the charged cluster in *H3* interacts with a charged head-groups of SDS at the rim of the hemi-micelle. Thus, SAXS models and HDX-MS exchange patterns can be reconciled but are not directly comparable due to the large difference in sensitivity where HDX-MS detects binding of single SDS molecules and SAXS only detects larger clusters of SDS. However, by combining these two complementary techniques, it is possible to achieve great insight into both specific interactions and overall structure. SAXS provide the overall low-resolution structure with the organization of the SDS and HDX-MS gives details on the specific parts of the protein that interacts with the SDS (hemi-) micelle.

4.2. Charge neutralization and aggregation

The net charge of TlL is computed to be + 18, −5, and −12 at pH 4.0, 6.0 and 8.0, respectively. Thus, we would expect a strong protein-SDS interaction at pH 4.0, where TlL has a positive overall charge and SDS is anionic. Electrostatic interactions clearly play a large role for TlL interactions with SDS, but the underlying mechanisms are complex. Thus, repulsion between SDS and TlL at pH 7.0 (which is expected to increase SDS resistance) is decreased by increasing salt concentrations, which provides shielding of the charges, but nonetheless still increases SDS resistance [61]. This was correlated with the decrease of cmc with increased salt concentration, which indicated that TlL was more sensitive towards single SDS molecules compared to SDS micelles [61]. It is not surprising in itself that protein and SDS interactions are pH sensitive; it has been observed that protein-surfactant systems can form large aggregates close to charge neutralization when mixing either positively charged proteins and anionic surfactant [16,62–64] or negatively charged proteins and cationic surfactants [7].

Furthermore, large aggregates around charge neutralization are a known phenomenon in surfactant/polymer systems with components of opposite charge [65–69]. These systems can be modelled in a similar way as our TlL series at pH 4.0 with components such as CS form factor, RF structure factor and a contribution from additionally larger cluster especially around charge neutralization [65–68]. The similarities of TlL:SDS complexes at pH 4.0 to surfactant/polymer complexes close to charge neutralization also stress that TlL is unfolded at this pH and therefore acts more as an extended polymer than a folded protein with a well-defined tertiary structure.

It is not only close to charge neutralization that SDS is known to induce aggregates. This is also the case for a number of amyloid-forming proteins such as Aβ, tau and α-synuclein [70]. Here aggregation is generally induced in a [SDS] below cmc where SDS molecules interact with more than one protein and thereby increase the local protein concentration at the interface of a shared micelle. For α-synuclein, a SAXS study was carried out to understand the complex formation and growth at various [SDS] [56]. This showed that in a narrow concentration range of 0.3 – 0.7 mM SDS, it was possible to induce aggregation that produced Thioflavin T binding fibrils growing as a RF chain of connected CS structures. At higher [SDS], a stable CS structure was formed with one α-synuclein monomer and one micelle. These different concentration regions are similar to what is seen for pH 6.0, where the dimer with a hemi-micelle forms in the cmc region and at higher concentrations rearranges to the stable CS structure.

4.3. Dimerization and hemi-micelle modelling

At pH 6.0 and 8.0, a dimer is induced at the lowest [SDS] (1.4 and 1.6 mM, respectively). The formation of a dimer at low [SDS] is also seen for ubiquitin [71] and the cellulose binding domain (CBD) of a *Cellulomonas fimi* xylanase [58]. For these proteins the dimer structure was bridged with small clusters of 4–7 SDS molecules sitting at the interface. It should be noted that while ubiquitin exists as a pure monomer in solution, as seen for TlL in this study, around 70 % of CBD exists in a dimeric state at the investigated concentration of 2 mg/mL CBD without SDS present. When more SDS is added to these systems, the proteins unfold and adopt the classical CS structure. As very few SDS molecules were bound, the shape and position of the SDS contribution were not optimized. However, this shows that similar structures with small SDS cluster/hemi-micelles have been observed with a much lower SDS binding number.

Additionally, other studies have reported structures at a low to intermediate [SDS] where the tertiary structure is not completely broken down, but nevertheless still supports micelle-like structures on the proteins. This has been revealed by pyrene fluorescence for example for the proteins zein [72], bromelain [73] and myoglobin [74]. Moreover, myoglobin also showed an initial ITC transition independent of protein concentration (binding number equal to zero) [74] and a tendency to form larger structures without a CS structure at an intermediate concentration of the biosurfactant rhamnolipid as seen by SAXS data (though the SAXS data were not modelled) [17]. This is similar to what we see for TlL, where the first ITC transition at pH 6.0 and 8.0 gave a binding number of 0 and −18 (Table 1), respectively, which could suggest that these kinds of complexes are also more common, but not well characterized due to the difficulty of obtaining detailed structural information for example through SAXS modelling. This is challenging even with SAXS data, as the contribution from the hemi-micelles structure to the SAXS signal is low (*e.g.* compared to contribution from CS structure), as seen from the relatively modest difference from 1.6 mM to 7.3 mM at pH 8.0 (Fig. 7A).

Furthermore, it should be noted that a study of TlL and the biosurfactants rhamnolipid (RL) and sophorolipid (SL) showed that dimers were induced at pH 6.0 and that SAXS data could be modelled with 5–10 molecules of either RL or SL at the dimer interface [75]. However, no complex formation was seen at pH 8.0, where SAXS data could be described as coexisting folded TlL monomers and RL/SL micelles. The modelling performed in this study also optimizes the size and shape of the lipid structure. However, ITC data did not show characteristic transitions, so it was not possible to extract binding numbers and moreover the lipids RL and SL are a mixture of molecules with slightly different structure, which makes the calculated contrast levels of the head and tail groups more uncertain. Because of this and the lack of suitable software, the structures could not be modelled with the same level of detail as our study where we were also able to vary the orientation and position of the hemi-micelle as part of the fitting.

To the best of our knowledge, the detailed modelling performed in the present work has not previously been done for protein hemi-micelles structures. However, similar approaches have been applied to model SAXS data of membrane proteins encapsulated in membrane mimicking entities consisting of various kinds of surfactants [47,48,76–79]. In these works, pseudo-atom types are used that consider the scattering contrast of the head and tail group of the surfactants. Then, a search is performed to optimize shape parameters such as the height and ellipticity of the structure. This is very similar to our approach of describing the SDS hemi-micelles with dummy atoms representing the head or tail group of SDS. One large difference between the two systems is that parts of a membrane protein must be in contact with the hydrophobic core to be stable, which limits the possible arrangement of the membrane mimicking entity relative to the protein. For the hemi-micelles there are more possible orientations and positions. In the study of protein-surfactants, especially membrane proteins, small-angle neutron scattering (SANS) is often used either alone [80] or in combination with SAXS [81,82]. With SANS it is possible to contrast match the lipids using a certain H_2O/D_2O ratio, which essentially gives a spectrum of only the protein. It is then possible to fit SAXS and SANS data using one model, which can make the results more robust. This approach could also be useful for particularly the hemi-micelle structures observed in our study, so the TlL and SDS contribution each could be studied (almost) alone through a H_2O/D_2O contrast variation. However, it should be noted that the contrast in SAXS is good for protein-surfactants systems, as the surfactants have a very different electron density compared to proteins and variation in the structure will therefore be clear. This is exemplified by the very different SAXS data seen at the various pH and [SDS] in this study.

4.4. Hemi-micelle structure as locked unfolding intermediate

A combination of rapid-reaction CD, SAXS, and Trp fluorescence data of SDS unfolding of β-lactoglobulin show that micelles bind rapidly to the protein initially, forming large asymmetric aggregates that quickly disintegrate to micelles bound to individual proteins [44]. Subsequently, the tertiary structure of β-lactoglobulin breaks down and it starts to wrap around the micelle. Similarly, a molecular dynamics study of titin and β-amylase together with SDS shows that micelles initially bind to the protein and then individual SDS molecules insert into the structure, thereby unraveling individual structural components before the entire protein is wrapped around the micelles [83]. In our study, only the equilibrium structures of TlL:SDS are considered, but detailed knowledge of the mechanism of unfolding could help understand the structures. It could be speculated that a micelle binds to TlL, but the activation energy for SDS molecules inserting in the TlL structures and thereby disrupting the structure is too large and therefore a stable complex is formed in the form of a dimer with a hemi-micelle. For pH 6.0, it is seen that the activation barrier can be overcome at higher [SDS] where the CS structure is adopted, but this does not happen at pH 8.0. The increased activation barrier at pH 8.0 that results in a higher kinetic stability has been discussed thoroughly in our earlier study [13]. The formation of a dimer with the hemi-micelle can be viewed as an alternative to the CS structure formed between stable proteins and SDS, which is feasible without unfolding as the SDS hemi-micelle has a large contact surface with the protein at the dimer interface that can stabilize the dimer by specifically binding to this species. This can be adopted at intermediate [SDS] (as for pH 6.0) or at SDS saturation (as for pH 8.0).

Despite the overall stabilization of TlL at pH 8.0 for high [SDS], our HDX-MS data and the known reduction in T_m from 72 °C to 40 °C in the presence of 10 mM SDS [7,13] show that the structure is somewhat destabilized upon addition of SDS (Fig. 10A). This effect has also been seen for other proteins such as cytochrome P450 2B4 where addition of nonionic surfactants produced a mix of local increased and reduced deuterium exchange [84]. Furthermore, a global decrease in deuterium uptake has been reported for ubiquitin when comparing 0 mM SDS to 1.4 mM SDS, indicating that SDS is binding to ubiquitin in a partially folded state [85]. A later study using SAXS showed that under these conditions ubiquitin is in fact participating in a complex of four ubiquitin and 41 SDS [71]. Thus, while ionic surfactants are thought to disrupt protein structure, they may still interact with specific substructures to shield them from exchange and in our case even stabilize a possible unfolding intermediate. Binding of individual SDS molecules

has also been invoked to explain a reduction in the rate of Cys-labelling kinetics of the membrane protein GlpG at low SDS mole fractions in mixed micelles of SDS and the non-ionic surfactant dodecyl maltoside [86].

5. Conclusions

We provide a structural analysis of the response of TlL to SDS over a range of pH values and in this process describe a dimeric hemi-micelle structure formed under slightly alkaline conditions. At pH 8.0, we identify specific SDS anchor points and show a constant level of destabilization above cmc although TlL remains folded. Furthermore, we have performed a detailed modelling of the hierarchical structures formed close to charge neutralization and find a clear progression in the hierarchy of aggregation, in which compaction is gradually reduced before the classical CS structure is formed at high [SDS].

We have extended our SAXS modelling to encompass a broad swathe of structures, ranging from large particles leading to a milky suspension via exceptionally stable hemi-micelle structures to classical CS structures. This modelling has been paired with an optimized form of HDX-MS that made it possible to investigate specific interactions even at high [SDS].

We hypothesized that the pH dependent stability arose from structurally distinct complexes of TlL:SDS, and this has been vindicated through SAXS and HDX-MS analysis.

Both modelling of SAXS data and the use of HDX-MS within protein-surfactant systems have been advanced compared to previous studies. The detailed modelling of SAXS has resulted in an unprecedented insight into the structure formation of SDS-protein systems. This modelling has employed recently developed structure factors for describing aggregation [41] and the novel modelling method based on Monte Carlo generated points and optimization by random searches, in combination with both high-resolution structure and analytical form factors for the CS structures, where both types of modelling have been done on absolute scale employing molecular and concentration restraints. Such modelling has been lacking in previous studies [16,20,71,87]. For HDX-MS on protein-surfactant systems, surfactant removal prior to MS analysis is crucial [27,28,33,34]. To the best of our knowledge, this is the first demonstration of automated SDS removal implemented in an HDX-MS set-up which applies reversed phase LC for analyte separation. The observations and analyses presented in this study are important to achieve a better understanding of protein-surfactant systems both from a fundamental and applied point of view. The analysis of similar systems of surfactant-stable proteins could elucidate if the structures of TlL:SDS complexes are representative of this class of protein complexes. A better understanding of this may enable the development of more stable protein formulations for the detergent industry as well as within e.g. food and personal care.

CRediT authorship contribution statement

Helena Østergaard Rasmussen: Investigation, Software, Formal analysis, Writing – original draft, Visualization. **Daniel T. Weltz Wollenberg:** Methodology, Formal analysis, Investigation, Writing – original draft, Visualization, Funding acquisition. **Huabing Wang:** Investigation. **Kell K. Andersen:** Investigation, Formal analysis. **Cristiano L. P. Oliveira:** Software, Formal analysis, Investigation, Methodology, Writing – review & editing. **Christian Isak Jørgensen:** Conceptualization, Supervision, Funding acquisition. **Thomas J. D. Jørgensen:** Writing – review & editing, Supervision, Funding acquisition. **Daniel E. Otzen:** Conceptualization, Writing – review & editing, Supervision, Funding acquisition. **Jan Skov Pedersen:** Conceptualization, Software, Writing – review & editing, Methodology, Supervision, Funding acquisition.

Declaration of Competing Interest

The authors declare that they have no known competing financial interests or personal relationships that could have appeared to influence the work reported in this paper.

Acknowledgement

We would like to thank Anne Søndergaard for assistance with SAXS measurements. DTWW gratefully acknowledge instrumental support from Bruker Daltonik.

Funding

The support from the Independent Research Fund Denmark, Natural Sciences (grant 8021-00133B (JSP)), Innovation Fund Denmark (grant 7038-00174B (DTWW)), Novozymes A/S (DTWW), CNPq research fellowship (grant 303001/2019-4(CLPO)), and from São Paulo Research Foundation (FAPESP) (2018/16092-5, 2016/24531-1 (CLPO)) are gratefully acknowledged.

Appendix A. Supplementary data

Supplementary data to this article can be found online at https://doi.org/10.1016/j.jcis.2021.12.188.

References

[1] P. Chandra, Enespa, R. Singh, P.K. Arora, Microbial lipases and their industrial applications: a comprehensive review, Microb. Cell Fact. 19 (1) (2020), https://doi.org/10.1186/s12934-020-01428-8.
[2] A. Houde, A. Kademi, D. Leblanc, Lipases and their industrial applications - An overview, Appl. Biochem. Biotechnol. 118 (1-3) (2004) 155–170.
[3] O. Kirk, T.V. Borchert, C.C. Fuglsang, Industrial enzyme applications, Curr. Opin. Biotechnol. 13 (4) (2002) 345–351.
[4] Research, G.V. *Industrial Enzymes Market Size, Share & Trends Analysis Report By Product (Carbohydrases, Proteases, Lipases, Polymerases & Nucleases), By Source, By Application, By Region, And Segment Forecasts, 2020 - 2027*. 2020; Available from: https://www.grandviewresearch.com/industry-analysis/industrial-enzymes-market.
[5] J. Adrio, A. Demain, Microbial Enzymes: Tools for Biotechnological Processes, Biomolecules 4 (1) (2014) 117–139.
[6] E. Jurado, V. Bravo, J. Núñez-Olea, R. Bailón, D. Altmajer-Vaz, M. Garía-Román, A. Fernández-Arteaga, Enzyme-based detergent formulas for fatty soils and hard surfaces in a continuous-flow device, J. Surfactants Deterg. 9 (1) (2006) 83–90.
[7] J.E. Mogensen, P. Sehgal, D.E. Otzen, Activation, inhibition, and destabilization of thermomyces lanuginosus lipase by detergents, Biochemistry 44 (5) (2005) 1719–1730.
[8] Y. Yu, J. Zhao, A.E. Bayly, Development of surfactants and builders in detergent formulations, Chin. J. Chem. Eng. 16 (4) (2008) 517–527.
[9] R. Berlemont, C. Gerday, in: Comprehensive Biotechnology, Elsevier, 2011, pp. 203–216, https://doi.org/10.1016/B978-0-444-64046-8.00017-3.
[10] A.M. Brzozowski, H. Savage, C.S. Verma, J.P. Turkenburg, D.M. Lawson, A. Svendsen, S. Patkar, Structural origins of the interfacial activation in Thermomyces (Humicola) lanuginosa lipase, Biochemistry 39 (49) (2000) 15071–15082.
[11] G. Fuentes, A. Ballesteros, C.S. Verma, Specificity in lipases: A computational study of transesterification of sucrose, Protein Sci. 13 (12) (2004) 3092–3103.
[12] C. Pinholt, M. Fanø, C. Wiberg, S. Hostrup, J.T. Bukrinsky, S. Frokjaer, W. Norde, L. Jorgensen, Influence of glycosylation on the adsorption of Thermomyces lanuginosus lipase to hydrophobic and hydrophilic surfaces, Eur. J. Pharm. Sci. 40 (4) (2010) 273–281.
[13] H. Wang, K.K. Andersen, P. Sehgal, J. Hagedorn, P. Westh, K. Borch, D.E. Otzen, pH Regulation of the Kinetic Stability of the Lipase from Thermomyces lanuginosus, Biochemistry 52 (1) (2013) 264–276.
[14] M.M. Nielsen et al., Unfolding of beta-sheet proteins in SDS, Biophys. J. 92 (10) (2007) 3674–3685.
[15] R. Pittrive, F.S. Impiombato, Binding of Sodium Dodecyl Sulphate to Various Proteins, Biochem. J. 109 (5) (1968) 825.
[16] H.O. Rasmussen et al., Unfolding and partial refolding of a cellulase from the SDS-denatured state: From beta-sheet to alpha-helix and back, Biochimica Et Biophysica Acta-General Subjects 1864 (1) (2020).

[17] H.G. Mortensen et al., Myoglobin and alpha-Lactalbumin Form Smaller Complexes with the Biosurfactant Rhamnolipid Than with SDS, Biophys. J. 113 (12) (2017) 2621–2633.
[18] J.D. Kaspersen, A. Søndergaard, D.J. Madsen, D.E. Otzen, J.S. Pedersen, Refolding of SDS-Unfolded Proteins by Nonionic Surfactants, Biophys. J. 112 (8) (2017) 1609–1620.
[19] K.K. Andersen, C.L. Oliveira, K.L. Larsen, F.M. Poulsen, T.H. Callisen, P. Westh, J. S. Pedersen, D. Otzen, The Role of Decorated SDS Micelles in Sub-CMC Protein Denaturation and Association, J. Mol. Biol. 391 (1) (2009) 207–226.
[20] Y. Sun, P.L.O. Filho, J.C. Bozelli, J. Carvalho, S. Schreier, C.L.P. Oliveira, Unfolding and folding pathway of lysozyme induced by sodium dodecyl sulfate, Soft Matter 11 (39) (2015) 7769–7777.
[21] K. Ibel, R.P. May, K. Kirschner, H. Szadkowski, E. Mascher, P. Lundahl, Protein-decorated micelle structure of sodium-dodecyl-sulfate–protein complexes as determined by neutron scattering, Eur. J. Biochem. 190 (2) (1990) 311–318.
[22] S. Chodankar, V.K. Aswal, J. Kohlbrecher, R. Vavrin, A.G. Wagh, Surfactant-induced protein unfolding as studied by small-angle neutron scattering and dynamic light scattering, J. Phys.-Condensed Matter. 19 (32) (2007), https://doi.org/10.1088/0953-8984/19/32/326102 326102.
[23] H. Maity, M. Maity, M.M.G. Krishna, L. Mayne, S.W. Englander, Protein folding: The stepwise assembly of foldon units, PNAS 102 (13) (2005) 4741–4746.
[24] M.J. Chalmers, S.A. Busby, B.D. Pascal, G.M. West, P.R. Griffin, Differential hydrogen/deuterium exchange mass spectrometry analysis of protein-ligand interactions, Expert Review of Proteomics 8 (1) (2011) 43–59.
[25] R.E. Iacob, S.R. Krystek, R.-C. Huang, H. Wei, L.i. Tao, Z. Lin, P.E. Morin, M.L. Doyle, A.A. Tymiak, J.R. Engen, G. Chen, Hydrogen/deuterium exchange mass spectrometry applied to IL-23 interaction characteristics: potential impact for therapeutics, Expert Review of Proteomics 12 (2) (2015) 159–169.
[26] M.B. Trelle, D.M. Dupont, J.B. Madsen, P.A. Andreasen, T.J.D. Jørgensen, Dissecting the Effect of RNA Aptamer Binding on the Dynamics of Plasminogen Activator Inhibitor 1 Using Hydrogen/Deuterium Exchange Mass Spectrometry, ACS Chem. Biol. 9 (1) (2014) 174–182.
[27] N.H. Joh et al., Modest stabilization by most hydrogen-bonded side-chain interactions in membrane proteins, Nature 453 (7199) (2008) 1266–U73.
[28] A. Khanal, Y. Pan, L.S. Brown, L. Konermann, Pulsed hydrogen/deuterium exchange mass spectrometry for time-resolved membrane protein folding studies, J. Mass Spectrom. 47 (12) (2012) 1620–1626.
[29] K.W. Anderson, E.S. Gallagher, J.W. Hudgens, Automated Removal of Phospholipids from Membrane Proteins for H/D Exchange Mass Spectrometry Workflows, Anal. Chem. 90 (11) (2018) 6409–6412.
[30] L.S. Busenlehner, S.G. Codreanu, P.J. Holm, P. Bhakat, H. Hebert, R. Morgenstern, R.N. Armstrong, Stress sensor triggers conformational response of the integral membrane protein microsomal glutathione transferase 1, Biochemistry 43 (35) (2004) 11145–11152.
[31] X. Zhang et al., Dynamics of the beta(2)-Adrenergic G-Protein Coupled Receptor Revealed by Hydrogen-Deuterium Exchange, Anal. Chem. 82 (3) (2010) 1100–1108.
[32] C.M. Hebling, C.R. Morgan, D.W. Stafford, J.W. Jorgenson, K.D. Rand, J.R. Engen, Conformational Analysis of Membrane Proteins in Phospholipid Bilayer Nanodiscs by Hydrogen Exchange Mass Spectrometry, Anal. Chem. 82 (13) (2010) 5415–5419.
[33] M. Rey, H. Mrázek, P. Pompach, P. Novák, L. Pelosi, G. Brandolin, E. Forest, V. Havlíček, P. Man, Effective Removal of Nonionic Detergents in Protein Mass Spectrometry, Hydrogen/Deuterium Exchange, and Proteomics, Anal. Chem. 82 (12) (2010) 5107–5116.
[34] O. Vadas, M.L. Jenkins, G.L. Dornan, J.E. Burke, Using Hydrogen-Deuterium Exchange Mass Spectrometry to Examine Protein-Membrane Interactions, in: Enzymology at the Membrane Interface: Interfacial Enzymology and Protein-Membrane Binding, 2017, pp. 143–172, https://doi.org/10.1016/bs.mie.2016.09.008.
[35] J.S. Pedersen, A flux- and background-optimized version of the NanoSTAR small-angle X-ray scattering camera for solution scattering, J. Appl. Crystallogr. 37 (3) (2004) 369–380.
[36] Y. Li, R. Beck, T. Huang, M.C. Choi, M. Divinagracia, Scatterless hybrid metal-single-crystal slit for small-angle X-ray scattering and high-resolution X-ray diffraction, J. Appl. Crystallogr. 41 (6) (2008) 1134–1139.
[37] E.M. Steiner, J. Lyngsø, J.E. Guy, G. Bourenkov, Y. Lindqvist, T.R. Schneider, J.S. Pedersen, G. Schneider, R. Schnell, The structure of the N-terminal module of the cell wall hydrolase RipA and its role in regulating catalytic activity, Proteins-Structure Function and Bioinformatics 86 (9) (2018) 912–923.
[38] J. Vilstrup, A. Simonsen, T. Birkefeldt, D. Strandbygård, J. Lyngsø, J.S. Pedersen, S. Thirup, Crystal and solution structures of fragments of the human leucocyte common antigen-related protein, Acta Crystallographica Section D-Structural Biology 76 (5) (2020) 406–417.
[39] M. Kotlarchyk, S.-H. Chen, Analysis of Small-Angle Neutron-Scattering Spectra from Polydisperse Interacting Colloids, J. Chem. Phys. 79 (5) (1983) 2461–2469.
[40] W. Burchard, K. Kajiwara, *Statistics of Stiff Chain Molecules .1. Particle Scattering Factor*, Proceedings of the Royal Society of London Series a-Mathematical and Physical Sciences 316 (1525) (1970) 185–199.
[41] A.H. Larsen, J.S. Pedersen, L. Arleth, Assessment of structure factors for analysis of small-angle scattering data from desired or undesired aggregates, J. Appl. Crystallogr. 53 (4) (2020) 991–1005.
[42] D. Franke, M.V. Petoukhov, P.V. Konarev, A. Panjkovich, A. Tuukkanen, H.D.T. Mertens, A.G. Kikhney, N.R. Hajizadeh, J.M. Franklin, C.M. Jeffries, D.I. Svergun, ATSAS 2.8: a comprehensive data analysis suite for small-angle scattering from macromolecular solutions, J. Appl. Crystallogr. 50 (4) (2017) 1212–1225.
[43] K. Manalastas-Cantos, P.V. Konarev, N.R. Hajizadeh, A.G. Kikhney, M.V. Petoukhov, D.S. Molodenskiy, A. Panjkovich, H.D.T. Mertens, A. Gruzinov, C. Borges, C.M. Jeffries, D.I. Svergun, D. Franke, ATSAS 3.0: expanded functionality and new tools for small-angle scattering data analysis, J. Appl. Crystallogr. 54 (1) (2021) 343–355.
[44] J.N. Pedersen, J. Lyngsø, T. Zinn, D.E. Otzen, J.S. Pedersen, A complete picture of protein unfolding and refolding in surfactants, Chem. Sci. 11 (3) (2020) 699–712.
[45] G.V. Jensen et al., Multi-Step Unfolding and Rearrangement of alpha-Lactalbumin by SDS Revealed by Stopped-Flow SAXS, Frontiers in Mol. Biosci. 7 (2020).
[46] J.S. Pedersen, Analysis of small-angle scattering data from colloids and polymer solutions: modeling and least-squares fitting, Adv. Colloid Interface Sci. 70 (1997) 171–210.
[47] A. Calcutta, C.M. Jessen, M.A. Behrens, C.L.P. Oliveira, M.L. Renart, J.M. González-Ros, D.E. Otzen, J.S. Pedersen, A. Malmendal, N.C. Nielsen, Mapping of unfolding states of integral helical membrane proteins by GPS-NMR and scattering techniques: TFE-induced unfolding of KcsA in DDM surfactant, Biochimica Et Biophysica Acta-Biomembranes 1818 (9) (2012) 2290–2301.
[48] J. Døvling Kaspersen, C. Moestrup Jessen, B. Stougaard Vad, E. Skipper Sørensen, K. Kleiner Andersen, M. Glasius, C.L. Pinto Oliveira, D.E. Otzen, J.S. Pedersen, Low-Resolution Structures of OmpA.DDM Protein-Detergent Complexes, ChemBioChem. 15 (14) (2014) 2113–2124.
[49] S.L. Harwood, J. Lyngsø, A. Zarantonello, K. Kjøge, P.K. Nielsen, G.R. Andersen, J. S. Pedersen, J.J. Enghild, Structural Investigations of Human A2M Identify a Hollow Native Conformation That Underlies Its Distinctive Protease-Trapping Mechanism, Mol Cell Proteomics 20 (2021), https://doi.org/10.1016/j.mcpro.2021.100090 100090.
[50] S. Maric, T.K. Lind, J. Lyngsø, M. Cárdenas, J.S. Pedersen, Modeling Small-Angle X-ray Scattering Data for Low-Density Lipoproteins: Insights into the Fatty Core Packing and Phase Transition, ACS Nano 11 (1) (2017) 1080–1090.
[51] Y. Hamuro, S.J. Coales, Optimization of Feasibility Stage for Hydrogen/Deuterium Exchange Mass Spectrometry, J. Am. Soc. Mass Spectrom. 29 (3) (2018) 623–629.
[52] W.K. Lim, J. Rösgen, S.W. Englander, Urea, but not guanidinium, destabilizes proteins by forming hydrogen bonds to the peptide group, PNAS 106 (8) (2009) 2595–2600.
[53] K.A. Rubinson, Practical corrections for p(H, D) measurements in mixed H2O/D2O biological buffers, Anal. Methods 9 (18) (2017) 2744–2750.
[54] D.T.W. Wollenberg, S. Pengelley, J.C. Mouritsen, D. Suckau, C.I. Jørgensen, T.J.D. Jørgensen, Avoiding H/D Scrambling with Minimal Ion Transmission Loss for HDX-MS/MS-ETD Analysis on a High-Resolution Q-TOF Mass Spectrometer, Anal. Chem. 92 (11) (2020) 7453–7461.
[55] O. Glatter, New Method for Evaluation of Small-Angle Scattering Data, J. Appl. Crystallogr. 10 (Oct1) (1977) 415–421.
[56] L. Giehm et al., SDS-Induced Fibrillation of alpha-Synuclein: An Alternative Fibrillation Pathway, J. Mol. Biol. 401 (1) (2010) 115–133.
[57] K.M. Gonçalves, L.R.S. Barbosa, L.M.T.R. Lima, J.R. Cortines, D.E. Kalume, I.C.R. Leal, L.S. Mariz e Miranda, R.O.M. de Souza, Y. Cordeiro, Conformational dissection of Thermomyces lanuginosus lipase in solution, Biophys. Chem. 185 (2014) 88–97.
[58] C. Hojgaard et al., Can a Charged Surfactant Unfold an Uncharged Protein?, Biophys J . 115 (11) (2018) 2081–2086.
[59] P. Kunzmann, K. Hamacher, Biotite: a unifying open source computational biology framework in Python, BMC Bioinf. 19 (1) (2018), https://doi.org/10.1186/s12859-018-2367-z.
[60] S. Santini, J.M. Crowet, A. Thomas, M. Paquot, M. Vandenbol, P. Thonart, J.P. Wathelet, C. Blecker, G. Lognay, R. Brasseur, L. Lins, B. Charloteaux, Study of Thermomyces lanuginosa Lipase in the Presence of Tributyrylglycerol and Water, Biophys. J . 96 (12) (2009) 4814–4825.
[61] M. Fano, M. van de Weert, E.H. Moeller, N.A. Kruse, S. Frokjaer, Ionic strength-dependent denaturation of Thermomyces lanuginosus lipase induced by SDS, Arch. Biochem. Biophys. 506 (1) (2011) 92–98.
[62] S. Magdassi, Y. Vinetsky, P. Relkin, Formation and structural heat-stability of beta-lactoglobulin/surfactant complexes, Colloids Surf. B-Biointerf. 6 (6) (1996) 353–362.
[63] A.K. Moren, A. Khan, Surfactant hydrophobic effect on the phase behavior of oppositely charged protein and surfactant mixtures: Lysozyme and sodium alkyl sulfates, Langmuir 14 (24) (1998) 6818–6826.
[64] D.E. Otzen, L.W. Nesgaard, K.K. Andersen, J.H. Hansen, G. Christiansen, H. Doe, P. Sehgal, Aggregation of S6 in a quasi-native state by sub-micellar SDS, Biochimica Et Biophysica Acta-Proteins and Proteomics 1784 (2) (2008) 400–414.
[65] B. Plazzotta, E. Fegyver, R. Mészáros, J.S. Pedersen, Anisometric Polyelectrolyte/Mixed Surfactant Nanoassemblies Formed by the Association of Poly (diallyldimethylammonium chloride) with Sodium Dodecyl Sulfate and Dodecyl Maltoside, Langmuir 31 (26) (2015) 7242–7250.
[66] M. Amann, J.S. Diget, J. Lyngsø, J.S. Pedersen, T. Narayanan, R. Lund, Kinetic Pathways for Polyelectrolyte Coacervate Micelle Formation Revealed by Time-Resolved Synchrotron SAXS, Macromolecules 52 (21) (2019) 8227–8237.
[67] P. Buchold, M. Ram-On, Y. Talmon, I. Hoffmann, R. Schweins, M. Gradzielski, Uncommon Structures of Oppositely Charged Hyaluronan/Surfactant Assemblies under Physiological Conditions, Biomacromolecules 21 (9) (2020) 3498–3511.

[68] I. Hoffmann, M. Simon, M. Bleuel, P. Falus, M. Gradzielski, Structure, Dynamics, and Composition of Large Clusters in Polyelectrolyte-Surfactant Systems, Macromolecules 52 (6) (2019) 2607–2615.
[69] C. La Mesa, Polymer-surfactant and protein-surfactant interactions, J. Colloid Interface Sci. 286 (1) (2005) 148–157.
[70] D.E. Otzen, Amyloid Formation in Surfactants and Alcohols: Membrane Mimetics or Structural Switchers?, Curr Protein Pept. Sci. 11 (5) (2010) 355–371.
[71] H.G. Mortensen, D.E. Otzen, J.S. Pedersen, Ubiquitin forms conventional decorated micelle structures with sodium dodecyl sulfate at saturation, J. Colloid Interface Sci. 596 (2021) 233–244.
[72] N. Deo, S. Jockusch, N.J. Turro, P. Somasundaran, Surfactant interactions with zein protein, Langmuir 19 (12) (2003) 5083–5088.
[73] R. Bhattacharya, D. Bhattacharyya, Resistance of bromelain to SDS binding, Biochimica Et Biophysica Acta-Proteins and Proteomics 1794 (4) (2009) 698–708.
[74] K.K. Andersen, P. Westh, D.E. Otzen, Global study of myoglobin-surfactant interactions, Langmuir 24 (2) (2008) 399–407.
[75] J.K. Madsen, J.D. Kaspersen, C.B. Andersen, J. Nedergaard Pedersen, K.K. Andersen, J.S. Pedersen, D.E. Otzen, Glycolipid Biosurfactants Activate, Dimerize, and Stabilize Thermomyces lanuginosus Lipase in a pH-Dependent Fashion, Biochemistry 56 (32) (2017) 4256–4268.
[76] S. Maric, N. Skar-Gislinge, S. Midtgaard, M.B. Thygesen, J. Schiller, H. Frielinghaus, M. Moulin, M. Haertlein, V.T. Forsyth, T.G. Pomorski, L. Arleth, Stealth carriers for low-resolution structure determination of membrane proteins in solution, Acta Crystallographica Section D-Structural Biol. 70 (2) (2014) 317–328.
[77] J. Pérez, A. Koutsioubas, Memprot: a program to model the detergent corona around a membrane protein based on SEC-SAXS data, Acta Crystallographica Section D-Biological Crystallography 71 (1) (2015) 86–93.
[78] N. Skar-Gislinge, S.A.R. Kynde, I.G. Denisov, X. Ye, I. Lenov, S.G. Sligar, L. Arleth, Small-angle scattering determination of the shape and localization of human cytochrome P450 embedded in a phospholipid nanodisc environment, Acta Crystallographica Section D-Structural Biol. 71 (12) (2015) 2412–2421.
[79] D.S. Molodenskiy, H.D.T. Mertens, D.I. Svergun, An automated data processing and analysis pipeline for transmembrane proteins in detergent solutions, Sci. Rep. 10 (1) (2020), https://doi.org/10.1038/s41598-020-64933-1.
[80] A. Sanchez-Fernandez, C. Diehl, J.E. Houston, A.E. Leung, J.P. Tellam, S.E. Rogers, S. Prevost, S. Ulvenlund, H. Sjögren, M. Wahlgren, An integrative toolbox to unlock the structure and dynamics of protein-surfactant complexes, Nanoscale Adv. 2 (9) (2020) 4011–4023.
[81] T. Bengtsen, V.L. Holm, L.R. Kjølbye, S.R. Midtgaard, N.T. Johansen, G. Tesei, S. Bottaro, B. Schiøtt, L. Arleth, K. Lindorff-Larsen, Structure and dynamics of a nanodisc by integrating NMR, SAXS and SANS experiments with molecular dynamics simulations, Elife 9 (2020), https://doi.org/10.7554/eLife.56518.
[82] N.T. Johansen, M.C. Pedersen, L. Porcar, A. Martel, L. Arleth, Introducing SEC-SANS for studies of complex self-organized biological systems, Acta Crystallographica Section D-Structural Biol. 74 (12) (2018) 1178–1191.
[83] D. Winogradoff, S. John, A. Aksimentiev, Protein unfolding by SDS: the microscopic mechanisms and the properties of the SDS-protein assembly, Nanoscale 12 (9) (2020) 5422–5434.
[84] M.B. Shah, H.-H. Jang, P.R. Wilderman, D. Lee, S. Li, Q. Zhang, C.D. Stout, J.R. Halpert, Effect of detergent binding on cytochrome P450 2B4 structure as analyzed by X-ray crystallography and deuterium-exchange mass spectrometry, Biophys. Chem. 216 (2016) 1–8.
[85] G.F. Schneider, B.F. Shaw, A. Lee, E. Carillho, G.M. Whitesides, Pathway for Unfolding of Ubiquitin in Sodium Dodecyl Sulfate, Studied by Capillary Electrophoresis, J. Am. Chem. Soc. 130 (51) (2008) 17384–17393.
[86] D.E. Otzen et al., Cys-labeling kinetics of membrane protein GlpG: a role for specific SDS binding and micelle changes?, Biophys J . 120 (2021) 4115–4128.
[87] Y. Sun, P.L. Oseliero, C.L.P. Oliveira, alpha-Lactalbumin and sodium dodecyl sulfate aggregates: Denaturation, complex formation and time stability, Food Hydrocolloids 62 (2017) 10–20.